sustainability

MDPI

Article

Comparing Design Schemes and Infection Risk Assessment of Negative Pressure Isolation Cabin

Shuwen Zhou [1], Yixin Zan [1] and Xiaolong Liu [1,2,*]

[1] School of Mechanical Engineering and Automation, Northeastern University, Shenyang 110819, China; shwzhou@mail.neu.edu.cn (S.Z.); 2200457@stu.neu.edu.cn (Y.Z.)
[2] School of Mechanical Engineering, Ningxia Institute of Science and Technology, Shizuishan 753000, China
* Correspondence: liuxiaolong9191@163.com

Abstract: At present, various public health emergencies have forced a deeper study of measures to prevent infectious diseases. To prevent the spread of infectious diseases on large cruise ships, the use of negative pressure isolation cabins is an effective method. However, existing cruise ships rarely use negative pressure isolation cabins or use them with shortcomings such as unreasonable layout of air inlets, which do not effectively reduce the risk of infection for medical staff while isolating patients. To solve this problem, first, the method of active air interference and the principle of proximity of the fresh air outlet were examined in this paper, and four groups of optimization schemes were designed. Second, by analyzing the diffusion of droplets in three breathing modes (coughing, sneezing, and talking while wearing or not wearing a mask), the direction of droplets and the efficiency of pollutant discharge under the condition of coughing were compared. Finally, in this paper, the infection risk of contact transmission and aerosol transmission was optimized by using the linear quantitative evaluation method and MSDR method, respectively. The results showed that the auxiliary air intake layout of optimal scheme 2 can effectively reduce the risk of infection for medical personnel in negative pressure isolation cabins. This study provides a useful reference for the design and optimization of negative pressure isolation cabins in future cruise ships.

Keywords: assessment of infection risk; diffusion of droplets; isolation cabin; optimized design; wearing a mask

Citation: Zhou, S.; Zan, Y.; Liu, X. Comparing Design Schemes and Infection Risk Assessment of Negative Pressure Isolation Cabin. *Sustainability* **2023**, *15*, 12780. https://doi.org/10.3390/su151712780

Academic Editors: Matthew Johnson, Alireza Afshari and Jinhan Mo

Received: 28 July 2023
Revised: 18 August 2023
Accepted: 21 August 2023
Published: 23 August 2023

1. Introduction

In recent years, the development of the transportation industry has made the global movement of people and goods more convenient and frequent, and ocean cruise tourism has become one of the fastest growing travel modes. Sea travel, including cruise tourism, has increased the spread of various pathogens, particularly the spread of infectious diseases [1,2]. Studies have shown that respiratory infections on cruise ships are the most common cause of travel and crew visits [3]. Particles larger than 5 μm expelled by patients while speaking, coughing, or sneezing are generally considered to be droplet transmission, and particles smaller than 5 μm are classified as airborne transmission. The airborne transmission of viruses refers to the spread of infectious pathogens caused by droplets (aerosols) suspended in the air, allowing them to maintain infectivity over long distances and for a long time [4]. Recent outbreaks of SARS, MERS, and COVID-19 were caused by the spread of droplet aerosols, and prior to the outbreak of COVID-19, such infectious diseases frequently occurred on cruise ships, causing serious public health security incidents [5,6].

Due to the large capacity of passengers, the small internal space, the poor effect of ventilation, intensive personnel activities, and the majority of passengers being elderly, once infectious diseases occur on cruise ships, they can easily cause the spread of cascading epidemics [7,8]. For example, in the summer of 2009, the outbreak of influenza A(H1N1) on the large luxury cruise ship "Pacific Dawn" and the COVID-19 outbreak on the Diamond

Princess in 2020 were both caused by inadequate protection and the failure to take timely quarantine measures [9,10]. In the past three years, the Center for Disease Control and Prevention in Morgantown, West Virginia, has used a self-designed cough aerosol simulator to analyze the effect of patients wearing face masks on reducing the excretion of COVID-19 virus aerosols during coughing and has designed the corresponding experimental devices for verification [11]. In addition to personal precautions such as wearing masks, negative pressure isolation wards are the most effective facilities to control the source of infection and cut off the transmission routes. Diseases transmitted on cruise ships are mainly respiratory infections caused by droplets or aerosols, and every cruise ship should be equipped with medical isolation facilities [12].

The negative pressure isolation cabin has good sealing. When there is an epidemic of infectious diseases on the cruise ship, confirmed patients can be quickly isolated to prevent the further spread of the epidemic and ensure the safety of the cruise ship personnel. On 14 September 2014, the newly constructed negative pressure isolation room was officially opened at the home port of China's Tianjin Cruise Line. This negative pressure isolation room has functions such as rapid screening, X-ray detection, quarantine detention, and sample processing, which can minimize the spread of infectious diseases [13]. With the rapid development of computer hardware and software, more and more researchers are now using computational fluid dynamics (CFD) methods to analyze biological pollutants [14–17]. After the outbreak of SARS in 2003, many nonvirological and biological experts and scholars adopted numerical simulation methods to simulate and analyze the organization of viral transmission airflow and evaluate regional airflow [18–24].

The existing negative pressure isolation cabin was designed by adding a negative pressure ventilation system to an ordinary cabin. However, the complexity of the flow field in the negative pressure isolation cabin was not considered in the arrangement of the air inlets, resulting in the risk of infection still existing during the process of treating patients. To solve the above issues, the following contributions are made in this paper by using numerical simulations. (1) Based on the active interference airflow method, combined with the fresh air outlet proximity principle, four optimization schemes are proposed to reduce the infection risk of medical staff. (2) The droplet diffusion in the negative pressure isolation cabin of a large cruise ship was compared and analyzed under three conditions: coughing, talking, and sneezing, and the effectiveness of wearing masks was theoretically analyzed. (3) The risk of infection was assessed from both contact transmission and aerosol transmission. Finally, the feasibility of the optimization scheme is verified.

This paper comprises six sections. Section 2 describes the numerical simulation and boundary conditions. Section 3 compares and analyzes the effectiveness of wearing a mask under three working conditions. In Section 4, the optimized model is compared and analyzed. In Section 5, the risk of infection is assessed. Section 6 gives the conclusion of this paper.

2. Building of Optimization Models and Numerical Simulation

2.1. Building of Optimization Models

Due to the limited space available on cruise ships, negative pressure isolation cabins are designed to take up less space than negative pressure wards. Therefore, the negative pressure isolation cabin of the cruise ship is designed and analyzed by reference to the compartment of negative pressure ambulances. This design not only saves space but also achieves negative pressure isolation. The isolation cabin is basically the same structure as the ambulance cabin, including basic medical equipment, stretchers, seats, etc. Not only are two individuals, a caregiver and a patient accommodated, but the patient must be kept in isolation until the ship is docked without developing any other symptoms. This is important for older people with underlying medical conditions, as most cruise passengers are elderly. A large amount of medical equipment is arranged on the right side of the patient, including oxygen cylinders, ECG monitors, first aid kits, infusion hangers,

and more. Moreover, after a reasonable layout, it has little effect on the fluid and can be reasonably simplified.

Depending on the difficulty of the model and the characteristics of surface modeling, SolidWorks was selected to complete solid modeling, and the model was modified in combination with the modeling software Design Modeler of Ansys Workbench. The mesh division method is the Fluent Meshing mixed mesh division method, the surface mesh is a polyhedron, including boundary layer division, and the body mesh is a hexahedral mesh structure. Due to the complex internal structure of the negative pressure isolation cabin, a reasonable simplification was made during modeling. Considering that the structure of the mannequin has a certain influence on the local fluid, a curved solid model with a height of 170 mm was selected without gender being ignored. Regardless of the effect of the holes and grilles on the fluid, the air inlet adopts an approximate rectangular port, which is divided into groups of two; the size of a single port is 140 mm × 60 mm, the interval within the group is 80 mm, and the interval between the groups is 400 mm. To generate the wall backflow, the influence of the grating on the fluid is considered in the exhaust outlet. The single mouth size is 55 mm × 5 mm matrix grid, and the patient's mouth is elliptical: the long axis is 40 mm and the short axis is 12 mm. The fluid simulation analysis is completed by Fluent 2020R2. The established fluid domain model is shown in Figure 1.

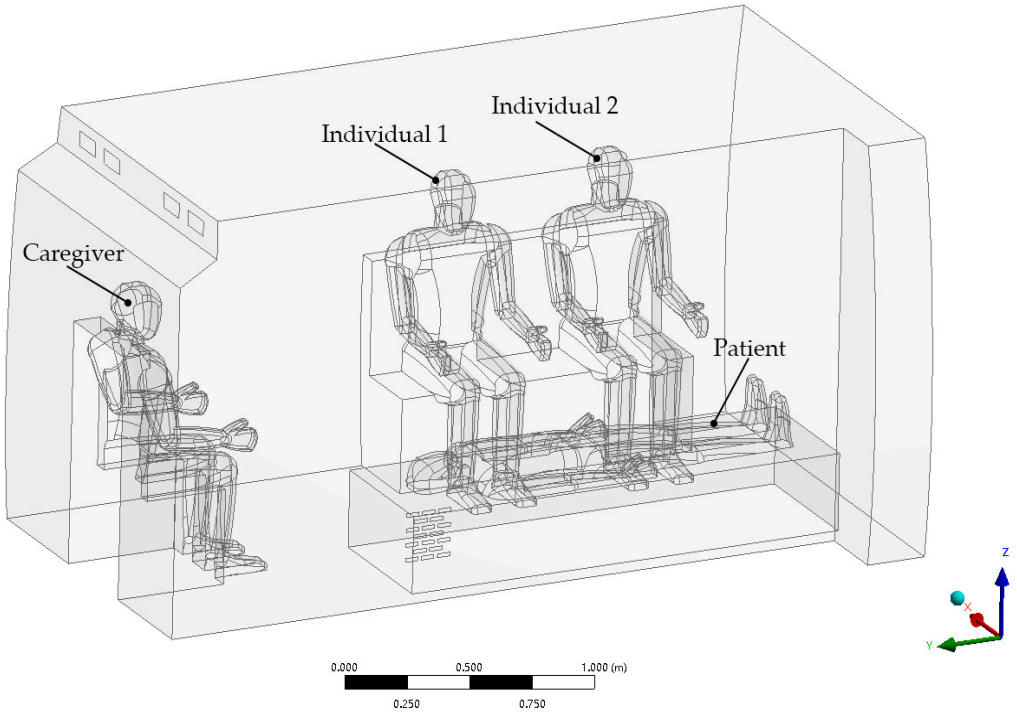

Figure 1. Negative pressure isolation tank watershed model.

Based on the characteristics of air flow and active interference methods, this paper proposes increasing the auxiliary inlet of the fresh air system to protect the individual, so that the breathing area of the individual is always in a clean, fresh air environment. Air intake above or behind the head of the individual and the two sets of seats form four combinations. The four schemes are air intake above the head of individual, air intake behind the head of individual, air intake above the head of caregiver + air intake behind the head of individual, and air intake behind the head of caregiver + air intake above the head of individual, as shown in Figure 2.

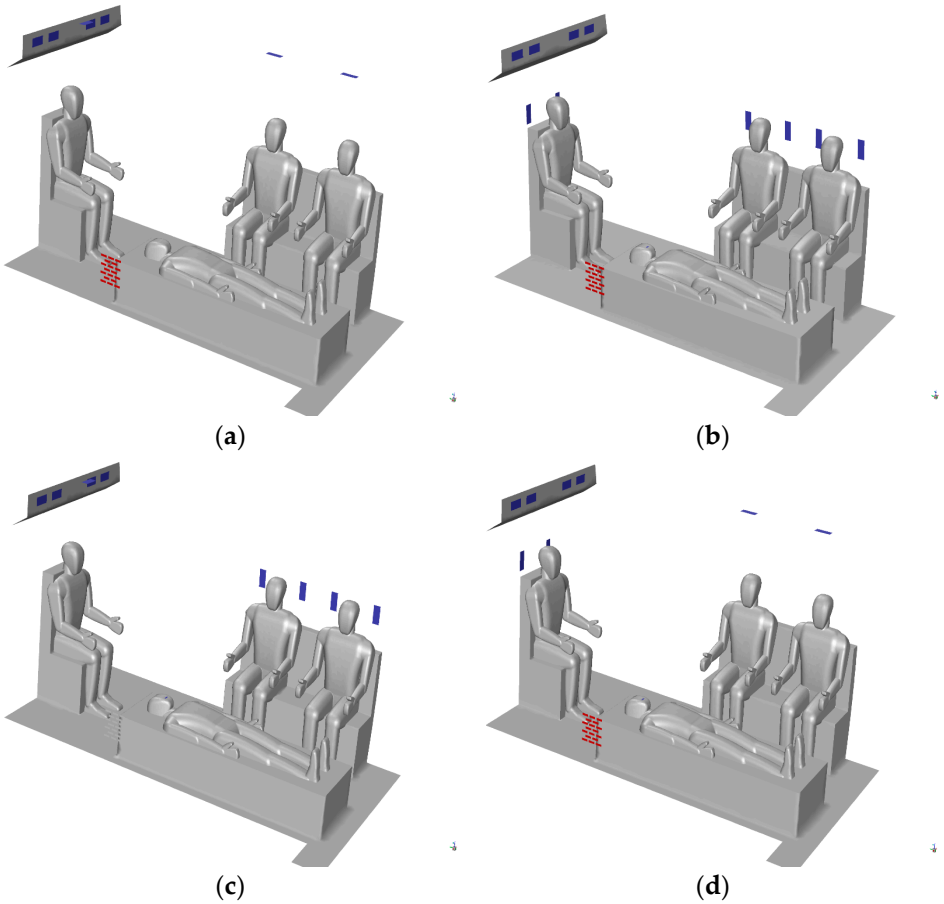

Figure 2. Distribution of the auxiliary air inlet (**a**) Optimization scheme 1; (**b**) Optimization scheme 2; (**c**) Optimization scheme 3; (**d**) Optimization scheme 4.

2.2. Numerical Simulation

2.2.1. Basic Control Equations

(1) Conservation of mass equations

Any flow problem satisfies the conservation law: the increase in mass per unit time in a fluid cell is the same as the net mass flowing into the cell in the same time interval [25]. Following this law, the general form of the mass conservation equation shown in Equation (1) can be obtained:

$$\frac{\partial \rho}{\partial t} + \frac{\partial}{\partial x_i}(\rho u_i) = S_m \tag{1}$$

where ρ is the density of the fluid; t is time; u is the velocity vector of the fluid; S_m is the source term.

(2) Momentum conservation equation

The flow of any flow system complies with the law of momentum conservation. According to Newton's second law, the external cooperative force on a fluid element is the rate of change of its momentum with time [25].

From this, the expression of the momentum conservation equation that can be obtained in the three directions of x, y, and z is:

$$\left.\begin{array}{l} \frac{\partial(\rho u)}{\partial t} + \mathrm{div}(\rho u U) = \frac{\partial p}{\partial x} + \frac{\partial \tau_{xx}}{\partial x} + \frac{\partial \tau_{yx}}{\partial x} + \frac{\partial \tau_{zx}}{\partial x} + F_x \\ \frac{\partial(\rho v)}{\partial t} + \mathrm{div}(\rho v U) = \frac{\partial p}{\partial y} + \frac{\partial \tau_{xy}}{\partial y} + \frac{\partial \tau_{yy}}{\partial y} + \frac{\partial \tau_{zy}}{\partial y} + F_y \\ \frac{\partial(\rho w)}{\partial t} + \mathrm{div}(\rho w U) = \frac{\partial p}{\partial z} + \frac{\partial \tau_{xz}}{\partial z} + \frac{\partial \tau_{yz}}{\partial z} + \frac{\partial \tau_{zz}}{\partial z} + F_z \end{array}\right\} \tag{2}$$

where p represents the pressure on the fluid microbody; τ_{ij} indicates surface stress; u, v, and w represent the velocity in the three directions of x, y, and z, respectively; F_x, F_y, and F_z refer to the physical strength on the microbody.

(3) Equation of energy conservation

When heat exchange is included in a fluid system, it must comply with the equation of energy conservation. This law is the first law of thermodynamics: the work done by the fluid microelement by physical or surface force and its own net heat flux is equal to the increase in the internal energy of the microelement. The equation is expressed as follows:

$$\frac{\partial(\rho T)}{\partial t} + \mathrm{div}\left(\rho \vec{u} T\right) = \mathrm{div}\left(\frac{k}{c_p}\mathrm{grad}T\right) + S_T \quad (3)$$

where T represents temperature; S_T represents the internal heat source of the fluid and the part of the mechanical energy of the fluid that is converted into heat energy due to viscous action; c_p indicates the specific heat capacity; k represents the heat transfer coefficient of the fluid.

2.2.2. Boundary Conditions

In this study, the DPM model is mainly used to simulate the movement of droplet aerosol particles generated by respiratory methods such as coughing by patients, and the simulation is a transient flow field. However, a steady-state result should be obtained before analysis of the transient flow field. The parameter of the steady-state calculation is shown in Table 1.

Table 1. Parameter settings for steady-state calculation.

Parameter	Value
solver type	Pressure-Based
energy equation	ON
gravity	9.81
turbulence model	RNG k-ε
solve method	SIMPLEC
discrete format	Second Order Upwind
initialization	Standard Initialization (inlet)

When using Fluent software for the simulation calculation, the same boundary conditions need to be added for each working condition as follows: the air inlet of the isolation cabin of a large cruise ship is the inlet boundary condition. The number of air changes in the isolation cabin of the cruise ship is set to 20 times /h, the volume of the fluid domain measured by Fluent is 7.208255 m^3, the size of the four air intake port of the air conditioner is 140 mm × 60 mm, and the minimum inlet wind speed can be obtained, and the inlet wind speed v = 1.5 m/s is finally determined. In the case of low temperature influence, the temperature is set at 21 °C combined with the air conditioning gear and human comfort. Hydraulic diameter D = 84 mm. Turbulence intensity I = 5.20%. At the same time, the temperature of the medical staff is taken into account, the temperature parameter for all human bodies in the isolation cabin is set to 28 °C, the patient's mouth temperature at 37 °C, and other default parameters can be selected. Set the outlet to the pressure outlet. The total pressure parameter is set to −30 Pa, and the direction is the vertical outlet surface.

The DPM model is used to simulate the movement of aerosol particles produced by respiratory patterns such as coughing. Common respiratory behaviors such as sneezing, coughing, and talking are the main ways of virus transmission and the main source of aerosol particles from droplets. According to the data of droplet particles generated by different breathing modes, the fixed values within each parameter interval are selected and the Rosin–Rammler [26] distribution is used for simulation. In the numerical calculation, two conditions are considered: without a mask and wearing a mask, and the particle

temperature is lowered to 30 °C when wearing a mask. The particle velocity is automatically corrected by the resistance of DEFINE_DPM_DRAG macro in the unmasked condition. Other important parameters related to droplets are shown in Table 2 [27–31].

Table 2. Parameters of droplets.

Parameter	Cough	Sneeze	Talk
flow rate (kg/s)	2.09×10^{-10}	2.09×10^{-10}	1×10^{-11}
particle size range (peak) (μm)	1~100 (90)	1~340 (210)	1~50 (30)
rate of incidence (m/s)	10	35	3.5
spray time (s)	0.4	0.4	2
particle size range (peak) (with mask) (μm)	1~100 (90)	1~120 (100)	1~50 (30)
traffic (with mask) (kg/s)	5.2×10^{-11}	5.2×10^{-11}	2.5×10^{-12}

In order to ensure the effectiveness of the simulation of wearing masks, a double-layer non-woven mask was selected for calculation [28]. The fiber diameter of the mask material is 227 μm, the layer spacing is 1 mm, and the fiber spacing is about 350 μm. In the Fluent DPM model, to refine the initial ejection of droplet aerosol particles, the UDF macro DEFINE_DPM_INJECTION_INIT is used to specify the change law of incident source position with time, including the change law of the initial state of the particle (such as particle size, speed, flow, temperature, etc.). When simulating wearing a mask, resistance is loaded with functional formulas through the macro DEFINE_DPM_DRAG. The air flow ejected by the patient is entered directly using the if condition function. In the Fluent simulation calculation, to better reflect the relationship between the discrete phase and the watershed model boundary, the four boundary conditions of patients, caregiver, individuals, and ground are set to Trap, the exit is set to Escape, and other boundaries such as walls are set to Reflect.

2.2.3. Grid Independence Verification

The data obtained in this paper comes from Fluent simulation software, so the validity of the data needs to be further studied. Tsz-Wun Tsang et al. [32] mentioned three common ways to validate a model: (1) using experimental or measurement results obtained in a real simulated environment; (2) making use of experimental or measurement results in the literature; (3) adopting the benchmark model. In this study, the method of grid independence verification [33] is used to illustrate the accuracy of the CFD model to ensure that the mesh size is reasonable and does not affect the calculation accuracy.

In order to ensure that there are no gaps, holes, or other problems in the grid, the free plane, multiple planes, overlapping plane, and skew rate (>0.85) are all 0, indicating that the model has a good structure. Then, according to the size of the special plane and the use occasion, the opposite grid is refined, the specific size is shown in Table 3.

Table 3. Main surface grid division size.

Parameter	Value (mm)
inlet	2~4
mouth	1~2
outlet	1~3
body	2~12
wall	40~50

The volume mesh size was selected as 100 mm, 80 mm, 60 mm, 50 mm, 40 mm, 30 mm, 25 mm, 20 mm, and 15 mm, respectively. In order to better explain the influence of the volume mesh size on the data results, the speed and pressure of the reference plane V plane at 15 mm above the patient were used for data analysis, as shown in Figure 3.

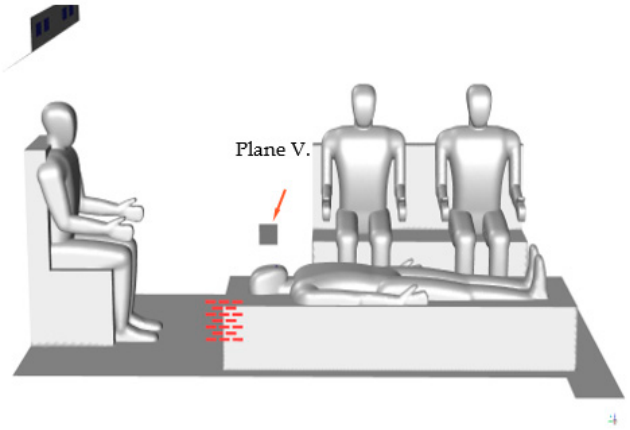

Figure 3. Reference plane setting.

After reasonable setting, simple boundary conditions and methods were used to obtain the velocity and pressure values of the reference plane V plane, and the results of grid independence verification were shown in Figure 4.

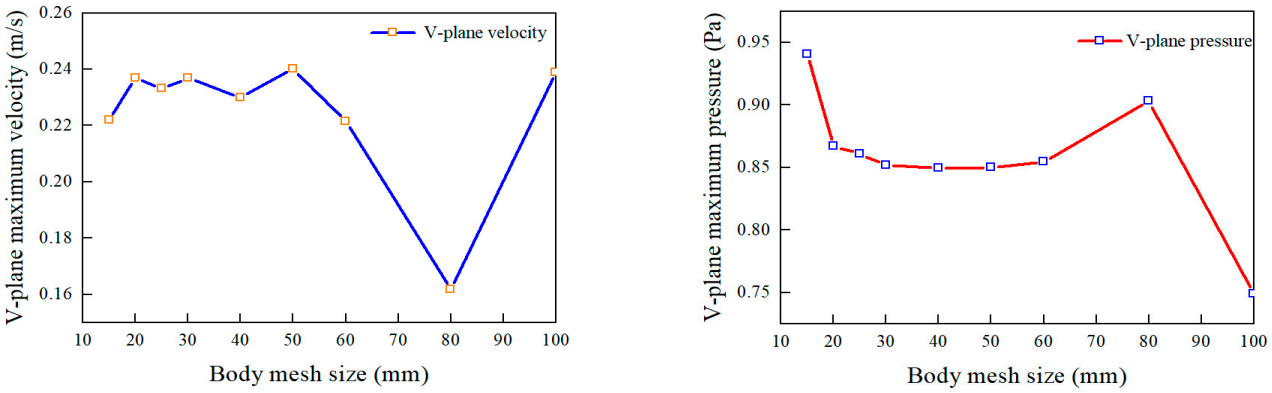

Figure 4. Grid independence verification (**a**) Reference plane parameter 1; (**b**) Reference plane parameter 2.

According to the result data of grid independence verification, combined with the selection principle of small data fluctuation and large mesh size, the volume mesh size is finally selected as 40 mm.

3. Comparison of Masks Worn under Three Working Conditions of the General Model

3.1. Cough

3.1.1. Residence Time of Discrete Droplets

(1) No masks

As shown in Figure 5, at 10 s, the droplets have moved to the rear of the isolation cabin. They move down from the top of the back of the isolation cabin under the influence of airflow and are mainly distributed around the patient near the medical equipment side. At this time, there are a small number of droplets in front of the caregiver and a very small number of droplets around the individual. At 120 s, the number of droplets suspended in the entire fluid domain is significantly reduced. Although more than half of the droplets have been exhausted or settled on the ground through the exhaust port, some droplets are evenly distributed throughout the fluid domain, indicating that the individuals and caregiver are still in a dangerous environment at this time.

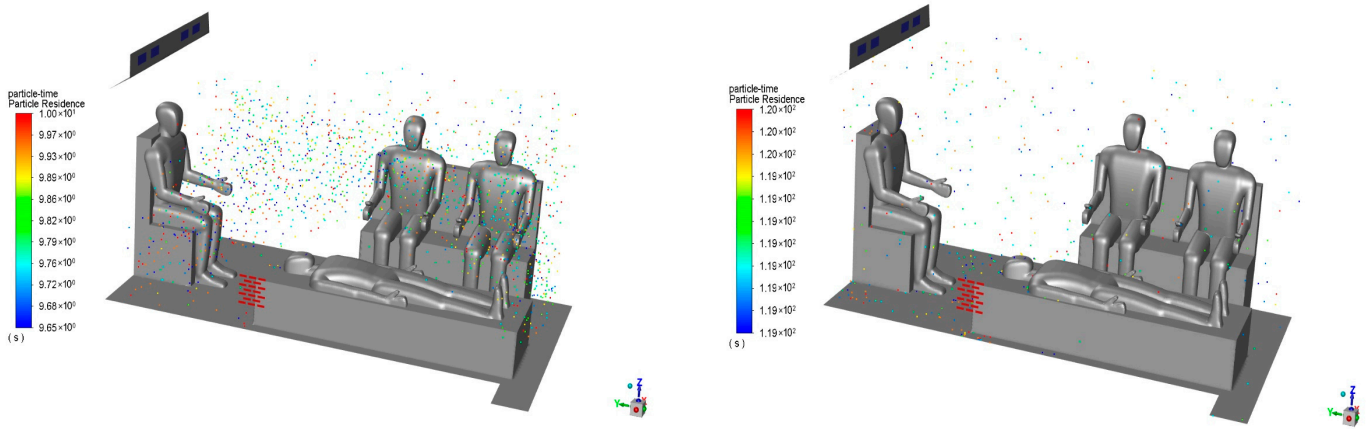

(**a**) (**b**)

Figure 5. Distribution of the particles of the droplets (cough without mask) (**a**) 10 s; (**b**) 120 s.

(2) Wearing a mask

As shown in Figure 6, at 10 s, a large number of droplets at the exit have been discharged. Some droplets are still in the drainage basin above the head of the patient and tend to discharge from the outlet. Nearly half of the droplets spread out on the right side of the caregiver and are evenly dispersed around the corner of the isolation cabin. A small fraction of droplets have reached the chest cavity of the caregiver, and the fastest-moving particles have reached the top of the caregiver's head. At 120 s, the droplets have not been significantly reduced, and there is a certain amount of particles around the caregiver and individuals. This indicates that droplets cannot be discharged quickly in a short time and the medical staff in the cabin are still at risk of infection.

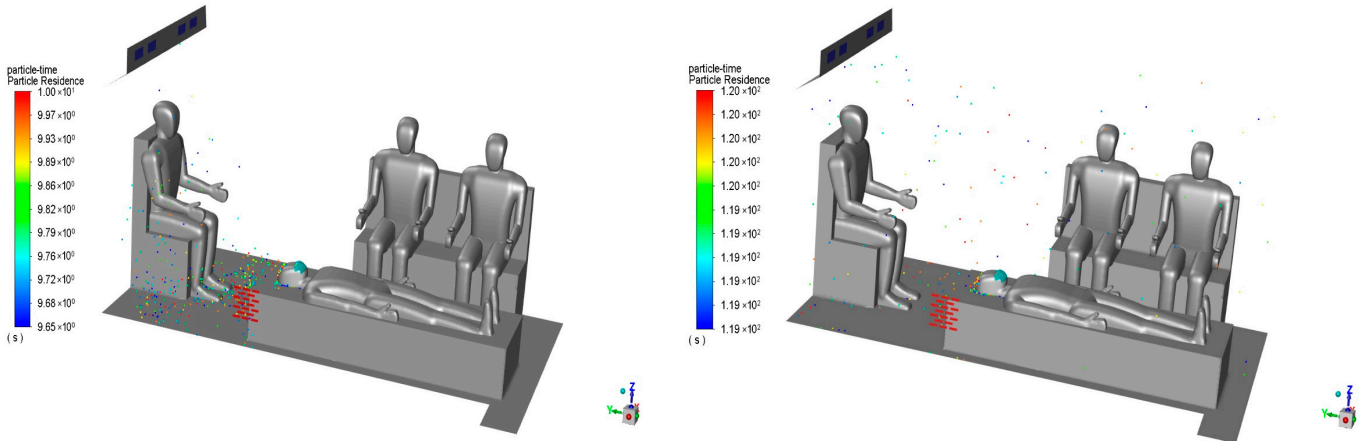

(**a**) (**b**)

Figure 6. Distribution of the particles of the droplets (cough with mask) (**a**) 10 s; (**b**) 120 s.

3.1.2. Distribution of Droplets of Different Sizes

The diameter range of droplets produced by coughing is 1~100 μm, and the main particle size value is 90 μm.

(1) No masks

As shown in Figure 7, the droplets at 1 s are still moving due to the force of the airflow generated by coughing, but due to the small airflow velocity near the patient's mouth and nose, and the large-size droplets of 63.2~90.1 μm are greatly affected by gravity, so no large displacement is produced. The droplets at 10 s are diffused in the watershed, and the large droplets with a large particle size of 16.4~27.1 μm in the remaining particles are mainly

distributed in the front of the isolation cabin, and most of them are located at the exit and on the ground.

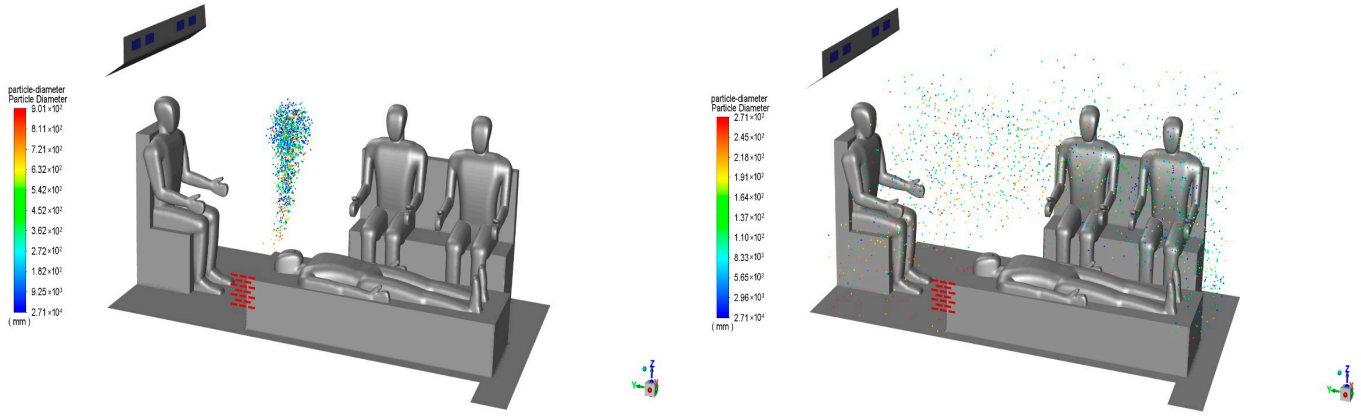

(**a**) (**b**)

Figure 7. Distribution of the particles of the droplets (cough without mask) (**a**) 1 s; (**b**) 10 s.

(2) Wearing a mask

As shown in Figure 8, the droplets at 1 s have an obvious stratification phenomenon, the larger droplets of 63.2~90.1 μm slide from the patient's face to the outlet direction, and the small droplets of small particle size of 0.271~27.2 μm float in the watershed. The large droplets at 10 s are basically in a stable state, and the main distribution in the watershed is the small droplets, and their diameter is less than 20 μm.

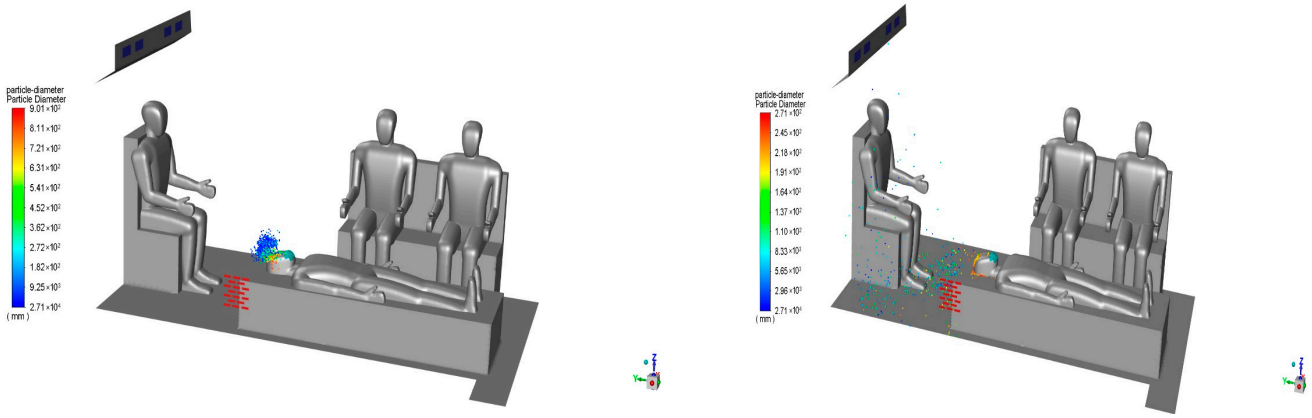

(**a**) (**b**)

Figure 8. Distribution of the particles of the droplets (cough with mask) (**a**) 1 s; (**b**) 10 s.

3.2. Sneeze

3.2.1. Discrete Droplets Particle Residence Time

(1) No masks

As shown in Figure 9, at 10 s, droplets are distributed throughout the watershed, some of which are discharged under the action of the flow field in the cabin, and some particles finally settle on the ground of the isolation cabin by gravity. Under the action of the mainstream, the droplets in the watershed move mainly in the area above the patient, near the wall of the isolation cabin, and the number of droplets near the medical staff is relatively small. At 120 s, most of the droplets have been discharged or settled on the ground, but a small number of particles are still floating in the basin inside the isolation cabin. It appears to be in a state of more before and less after, and continues to float near medical staff, so that medical staff is at risk of infection.

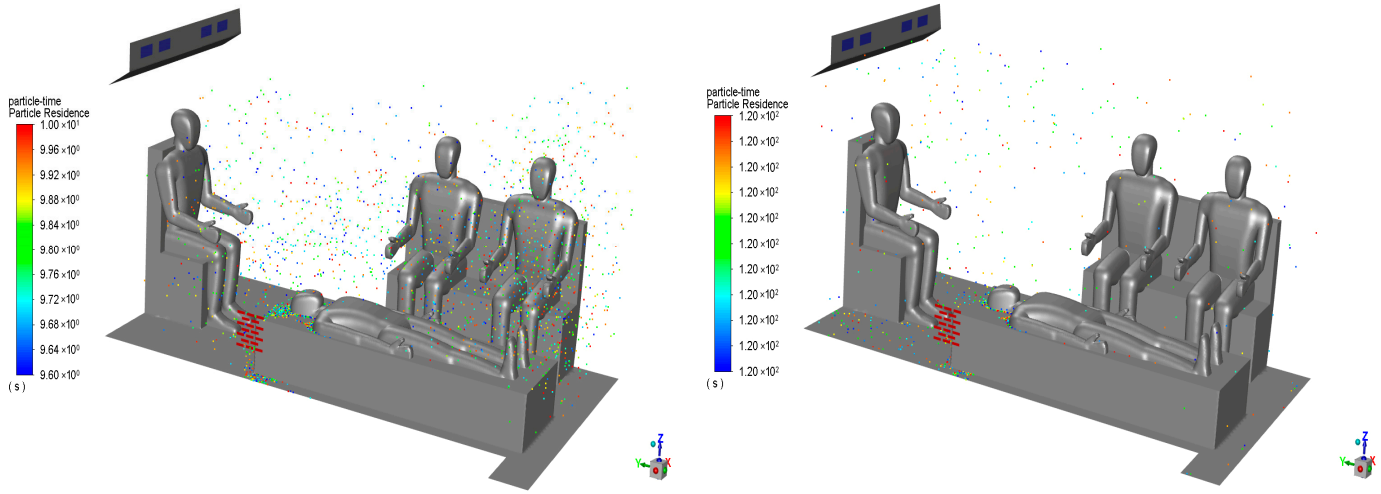

(**a**) (**b**)

Figure 9. Distribution of the particles of the droplets (sneezing without mask) (**a**) 10 s; (**b**)120 s.

(2) Wearing a mask

As shown in Figure 10, at 10 s, most of the droplets have been discharged from the outlet, and there is no obvious settlement on the stretcher of the patient's head. The remaining droplets eventually accumulate on the right side of the caregiver and move upward to the facial area. The risk of infection in caregiver is higher than that in other workers. At 120 s, only a few particles float throughout the fluid domain, droplets are present near caregiver and individuals, and most of the particles have been discharged.

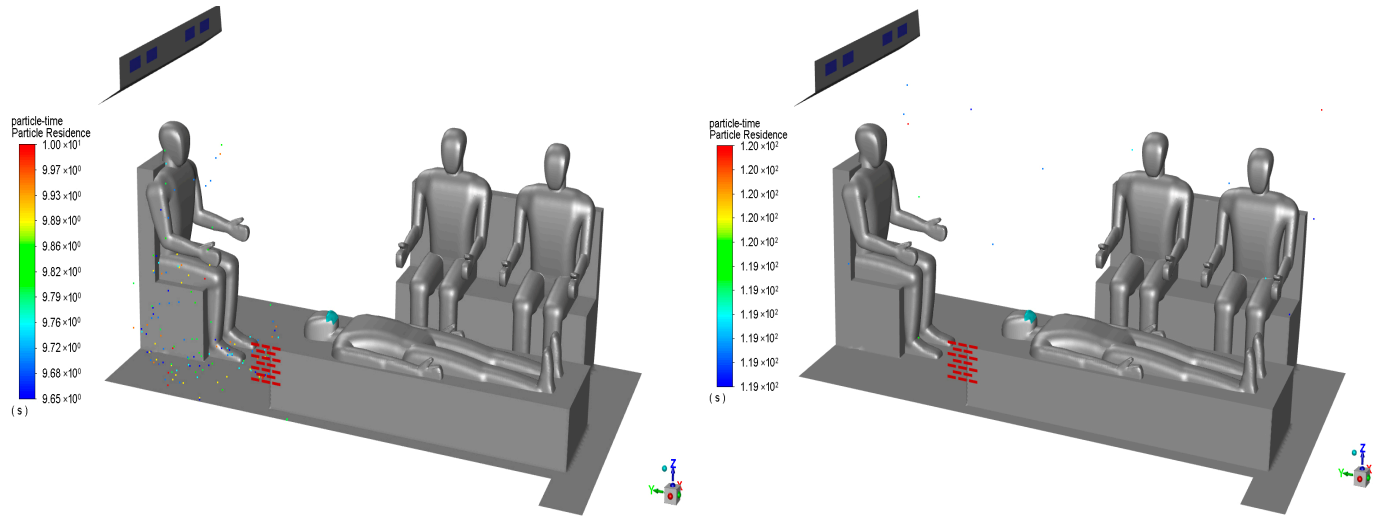

(**a**) (**b**)

Figure 10. Distribution of the particles of the droplets (sneezing with mask) (**a**) 10 s; (**b**) 120 s.

3.2.2. Distribution of Droplets of Different Sizes

Sneezing will produce many droplets, and compared to coughing and talking, droplets are much larger. Research has concluded that their diameter range is 1~340 μm, with most of the droplets being about 210 μm in diameter.

(1) No masks

As shown in Figure 11, the distribution of droplets at 1 s is clear. Droplets with a large particle size of 232~332 μm begin to fall near the patient's head, indicating that the mainstream does not have a significant effect on the droplets of large size. The droplets

with a small particle size of 0.271~99.7 μm are located in the top area of the isolation cabin. At 10 s, the watershed is full small of droplets, all of a diameter of less than 80 μm, and they float in the watershed under the action of air flow.

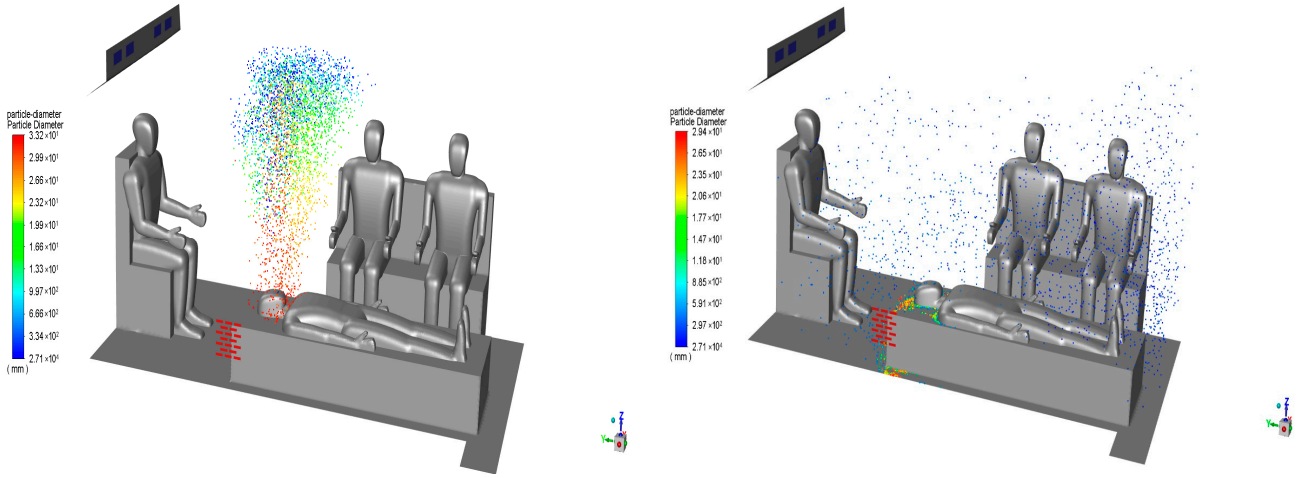

(**a**) (**b**)

Figure 11. Distribution of the particles of the droplets (sneezing without mask) (**a**) 1 s; (**b**) 10 s.

(2) Wearing a mask

As shown in Figure 12, the diameter of the droplets at 1 s is less than 7.45 μm, and are distributed in a lump shape with the movement of the air flow to the outlet. The droplets of 10 s do not appear to be distributed differently due to the different sizes of the droplets, and all of the droplets are mixed together and spread to the isolation cabin.

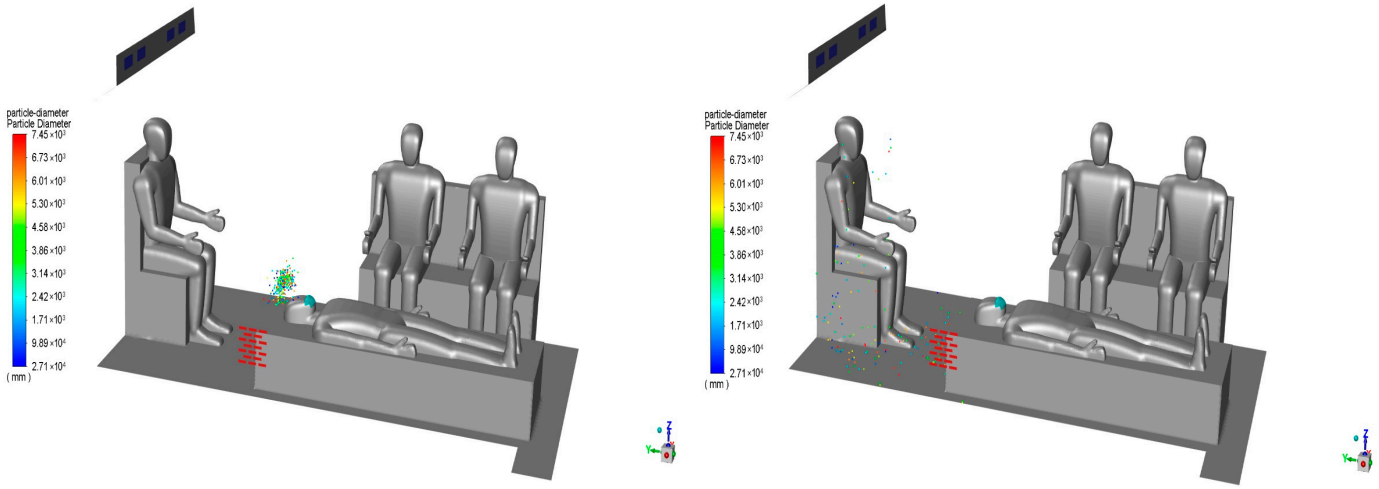

(**a**) (**b**)

Figure 12. Distribution of the particles of the droplets (sneezing with mask) (**a**) 1 s; (**b**) 10 s.

3.3. Talk

3.3.1. Discrete Droplets Particle Residence Time

(1) No masks

As shown in Figure 13, at 10 s, the two-second speaking process produces a very large number of droplets, and speaking generates airflow at a relatively low speed. Droplets do not reach the top of the isolation cabin and are mainly distributed around the caregiver under the influence of the mainstream. At this time, the caregiver is at high risk of infection. At 120 s, there are still many suspended droplets in the air, and fewer particles

settle on the ground, indicating that most droplets can have been discharged. But the suspended particles are evenly distributed in the watershed, which poses a greater threat to medical staff.

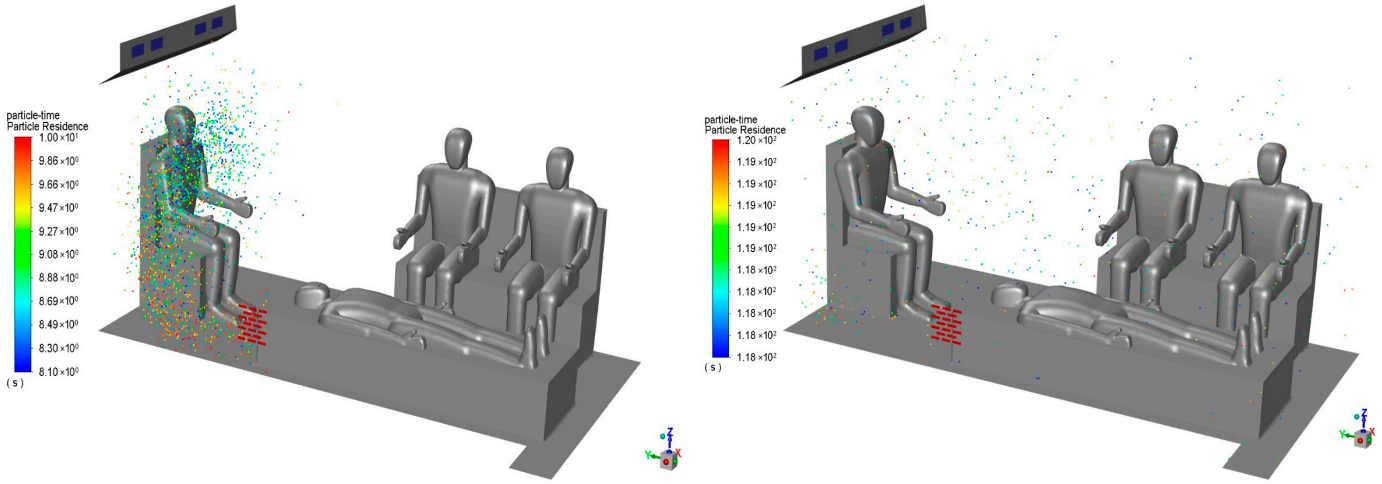

(**a**) (**b**)

Figure 13. Distribution of the particles of the droplets (talk without mask) (**a**) 10 s; (**b**) 120 s.

(2) Wearing a mask

As shown in Figure 14, the droplets at the exit decreased significantly at 10 s. Some of the droplets are near the floor of the isolation cabin. A small amount of droplets are dispersed around the caregiver and have reached the caregiver's face as far as possible. At this time, the risk of infection of the caregiver is increased and the individuals are not threatened. At 120 s, the droplets remaining in the air were not completely discharged. Although the amount is very small and far from the facial area of the medical staff, the effect of the air flow makes it possible to reach the breathing area of the medical staff at any time. The risk of infection cannot be ignored.

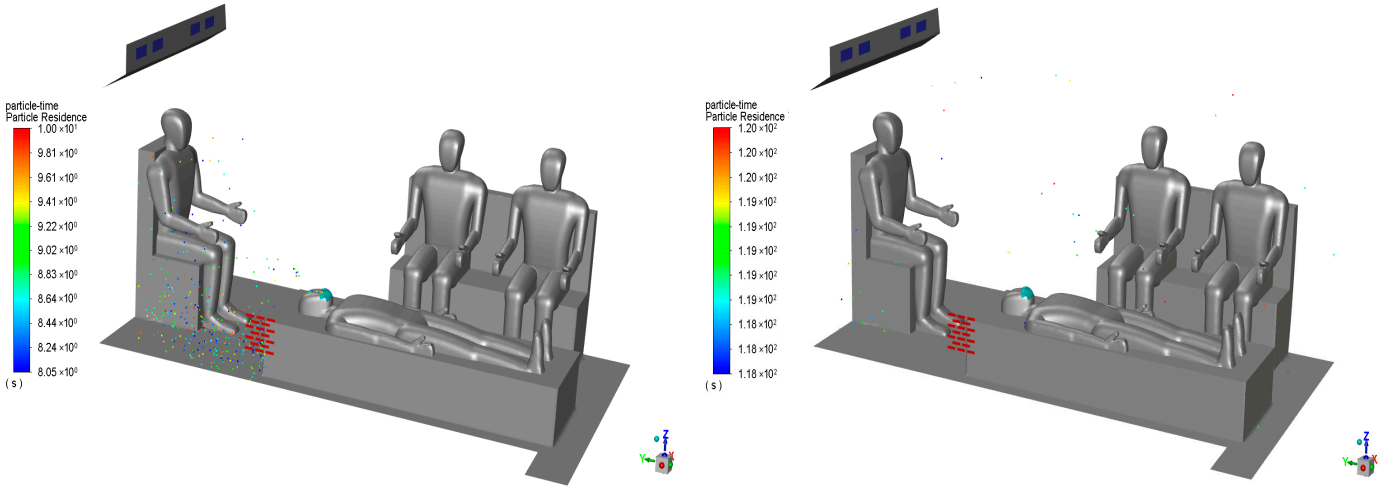

(**a**) (**b**)

Figure 14. Distribution of the particles of the droplets (talk with mask) (**a**) 10 s; (**b**) 120 s.

3.3.2. Distribution of Droplets of Different Sizes

Speaking, unlike coughing and sneezing, produces very small air currents and droplets. The diameter range of the selected droplets is 1~50 μm. Most droplets are about 30 μm in diameter.

(1) No masks

As shown in Figure 15, at 1 s, most droplets with a diameter below 20 μm move rapidly and dispersed. Droplets with larger particle sizes of 33.9~48.3 μm are near the mouth and nose of the patient. Droplets at 10 s are distributed near the outlet and caregiver, and droplets are mixed relatively evenly.

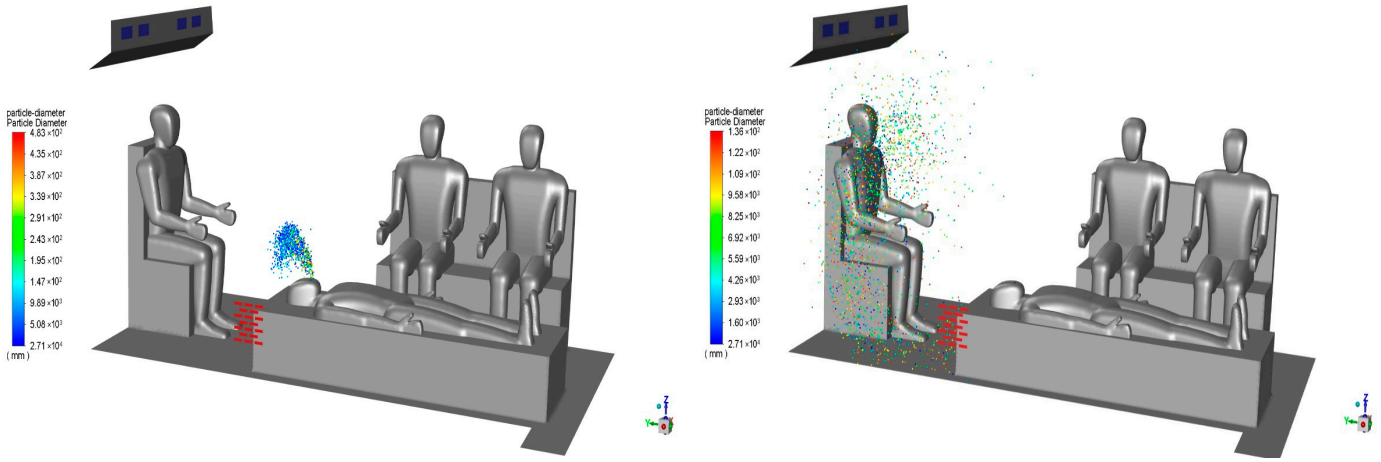

(**a**) (**b**)

Figure 15. Distribution of the particles of the droplets (talk without mask) (**a**) 1 s; (**b**) 10 s.

(2) Wearing a mask

As shown in Figure 16, the droplets move in the outlet direction at 1 s, and most of the droplets have a particle size value of less than 20 μm. There is a tendency to spread upward. At 10 s, some droplets are discharged from the outlet, resulting in a significant decrease in the number of droplets. At this time, a small number of large particle size droplets of 10.9~13.6 μm remain in the facial area of the patients. The particle size of the droplets in the basin is less than 13.6 μm.

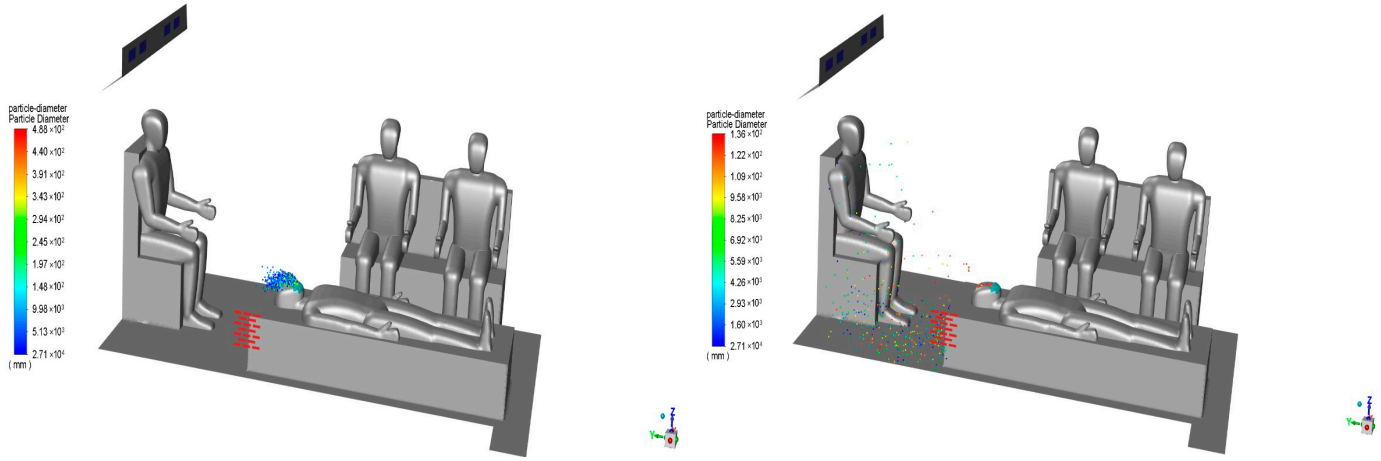

(**a**) (**b**)

Figure 16. Distribution of the particles of the droplets (talk with mask) (**a**) 1 s; (**b**) 10 s.

4. Comparison Analysis of the Optimized Model

In this paper, the four sets of optimization models adopt the active interference airflow method and are designed based on the principle of fresh air inlet. The optimization design only uses the most common cough in the new coronavirus for simulation. To better obtain the features of each scheme under the condition of wearing a mask or not, the two working conditions of wearing a mask and no mask are still used to compare and analyze the

location of droplets and the efficiency of sewage discharge, including being captured by medical staff and other walls, floating in the watershed, and discharged. According to the characteristics of the droplet particle size range produced under each working condition, the relationship between the droplets of different sizes and the five boundary conditions of patient, caregiver, individuals, ground, and outlet in the time dimension is determined.

4.1. Comparative Analysis of the Location of Droplets

4.1.1. Comparative Analysis of No Masks

As shown in Figure 17, a large number of droplets in each scheme are captured by each boundary. The large particle size of 50~70 μm has almost been discharged from the outlet in 10 s. Except for the second scheme, the patient boundary did not capture droplets in a short period of time, and except for the particles discharged from the outlet, the particle size captured at the remaining boundaries does not exceed 20 μm. Scheme 2 does not capture droplets after 60 s; the droplets of the four groups of schemes settled to the ground in the early stage and the outlet boundary is continuously discharged droplets, although the droplets settled in scheme 3 are relatively small, but not as good as scheme 2, and the number of droplets settled in the later stage of scheme 2 gradually decreased. Caregiver and individuals in the four groups catch droplets throughout the process, and although in small numbers, they are already a threat to medical staff.

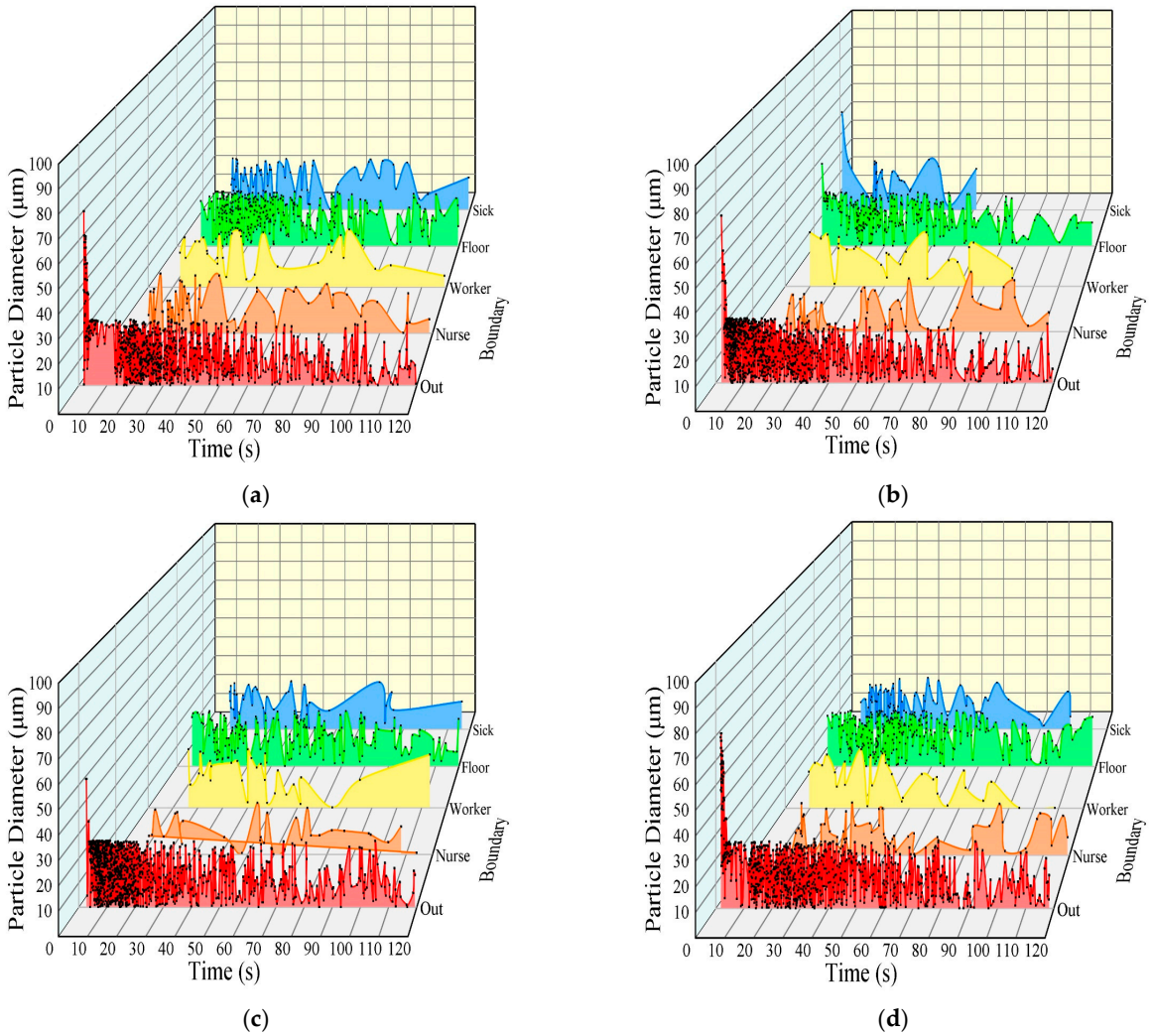

Figure 17. Final destination of droplets (no masks) (**a**) Optimization scheme 1; (**b**) Optimization scheme 2; (**c**) Optimization scheme 3; (**d**) Optimization scheme 4.

4.1.2. Comparative Analysis of Mask Use

As shown in Figure 18, affected by the mask, patients in all protocols instantly capture droplets and the particle size exceeds 50 μm. Schemes 1 and 4 capture relatively few droplets on the ground, and the most droplets adsorb on the surface of the caregiver in scheme 3. When the droplets are captured by the individual boundary, scheme 3 captures relatively more after 30 s, and the particle size range is 0~30 μm, while scheme 1 and scheme 4 do not capture droplets within 120 s. The export boundary can reflect the number and time point of droplets discharged by the isolation cabin within 120 s, scheme 1 and scheme 4 basically discharge a large number of droplets within 10 s, and particles larger than 20 μm have been discharged within 5 s, while scheme 2 and scheme 3 continue to discharge particles in the range of 0~20 μm for the entire time period.

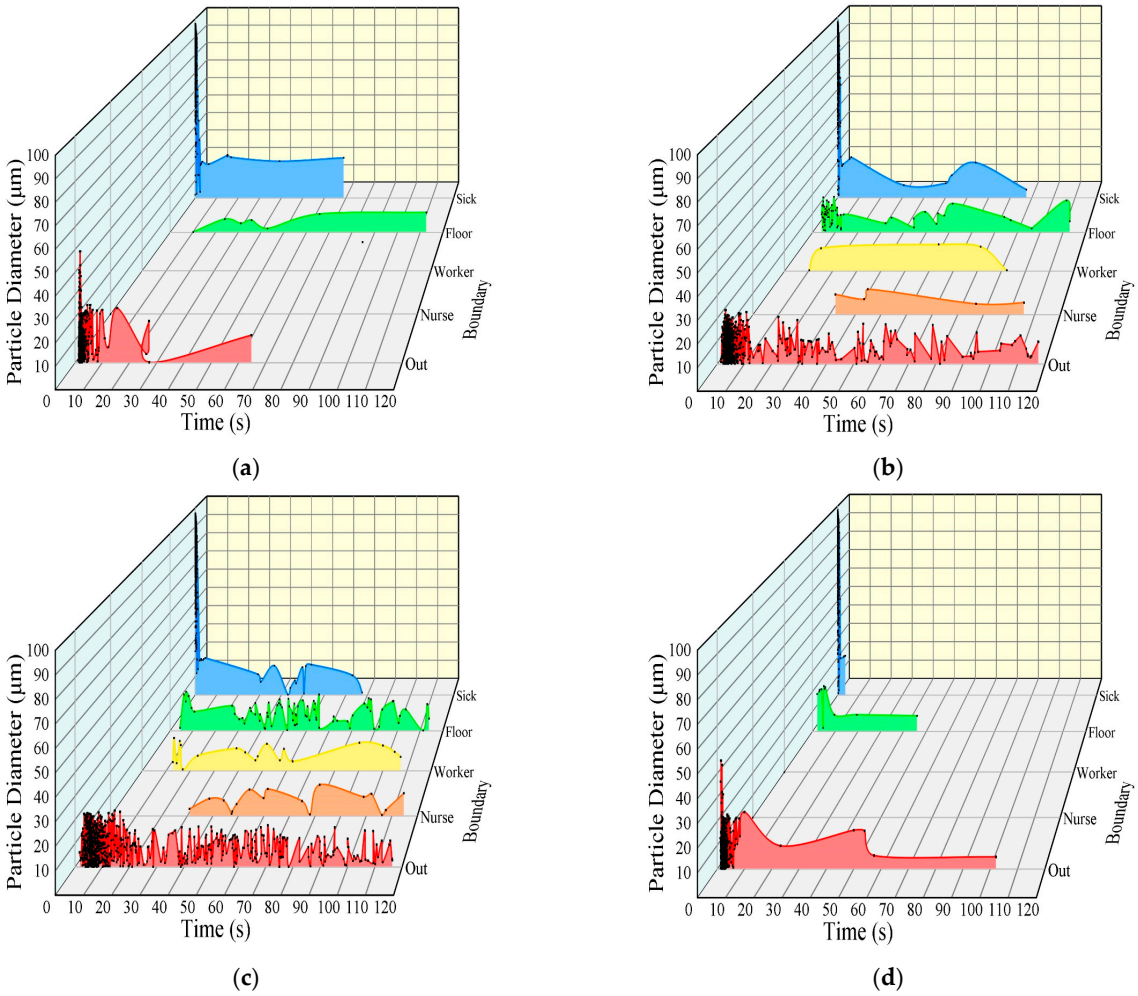

Figure 18. Final destination of droplets (with mask) (**a**) Optimization scheme 1; (**b**) Optimization scheme 2; (**c**) Optimization scheme 3; (**d**) Optimization scheme 4.

4.1.3. Comparative Analysis of Five Optimization Solutions

The purpose of the four optimization schemes is to actively interfere with the intensity and direction of airflow in the isolation cabin to affect the patient's breathing pattern and the movement of particles. In the general quarantine cabin model, seemingly stable and regular watersheds are not optimal.

As shown in Figure 19, the simulation result data from the four sets of optimization schemes and the general model simulation data are compared, and from the number of droplets captured on the body surface of medical personnel, it can be judged that schemes 1 and 4 perform well in mask mode, and both schemes reduce the probability of medical

staff carring the virus on the body surface. In the absence of masks, both schemes 2 and 3 can reduce the probability that medical staff carry the virus on the surface of their bodies. Patients can capture droplets under all working conditions, and droplets that settled on the floor of the negative pressure isolation cabin are also dangerous. Schemes 1, 3 and 4 for the mask-wearing condition are all reasonable, and schemes 2, 3 and 4 for the mask-free scenario are reasonable. From the perspective of the number of droplets discharged, all schemes in the mask-wearing mode are effective, and the maskless mode schemes 2 and 3 are effective.

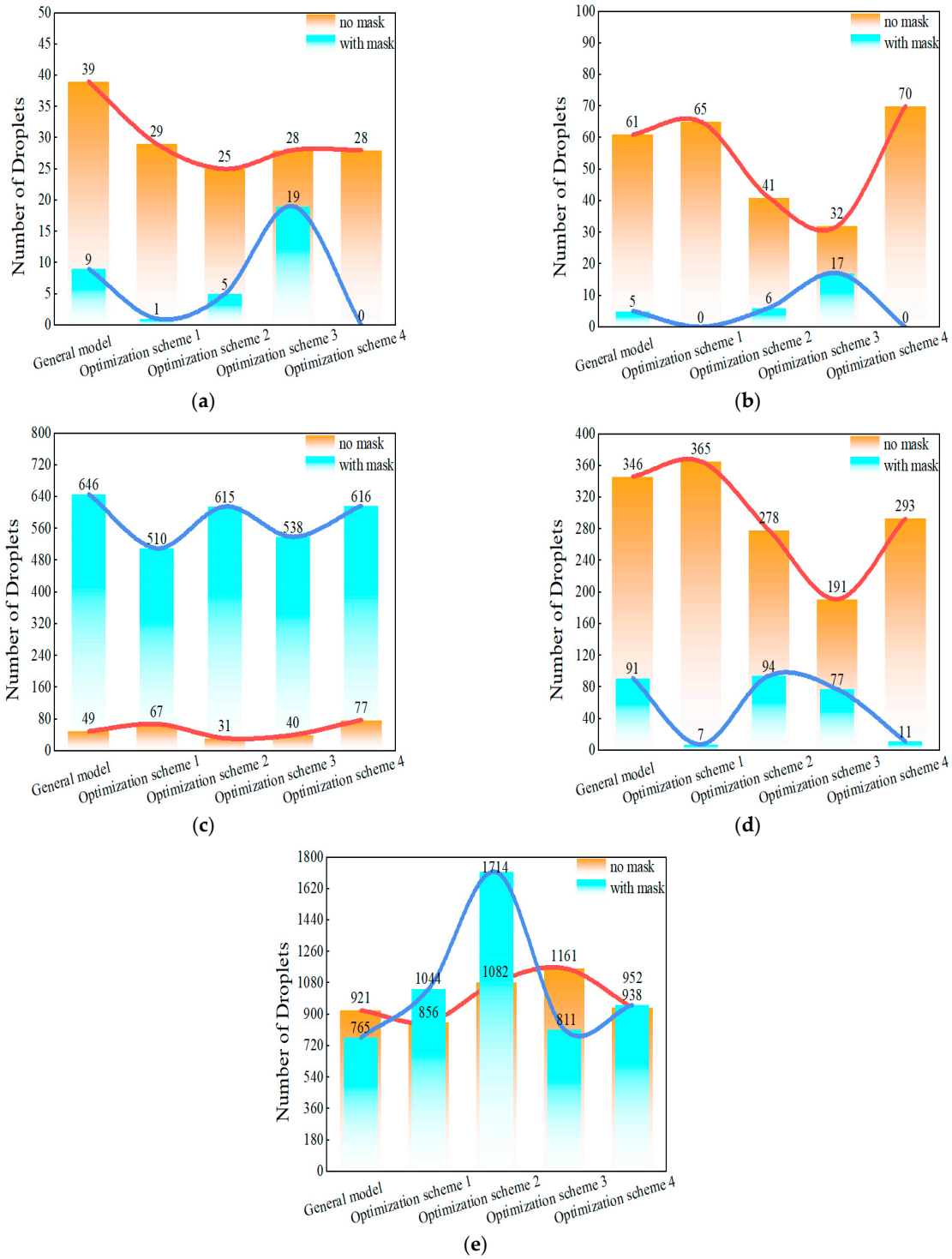

Figure 19. Statistics on the location of droplets: (**a**) Individual; (**b**) Caregiver; (**c**) Patient; (**d**) Floor; (**e**) Out.

4.2. Comparative Analysis of Sewage Efficiency

Discharge efficiency refers to the ability to discharge pollutants in a specific area through the input and outlet equipment, and the calculation formula of the discharge efficiency of pollutants at a certain point in time is as follows [34]:

$$\varepsilon_t = 1 - \frac{C_t}{C_0} \times 100\% \quad (4)$$

where C_0 is the initial concentration of pollutants in the region, kg/m^3. The C_t is the concentration of pollutants at the time of t, kg/m^3.

Using the above method, the concentration of the droplets dispersed in the total volume of t = 0.50 s and t = 120 s is calculated, and the efficiency of sewage discharge under mask-free and mask-wearing conditions is shown in Tables 4 and 5.

Table 4. Comparison of the efficiency of sewage discharge (cough without mask).

Name	General Model	Optimization Scheme 1	Optimization Scheme 2	Optimization Scheme 3	Optimization Scheme 4
t = 0.50 s droplets concentration(kg/m^3)	9.30×10^{-11}		9.30×10^{-11}		
t = 120 s droplets concentration(kg/m^3)	6.4690×10^{-12}	2.7620×10^{-12}	3.7796×10^{-12}	1.0031×10^{-11}	1.5264×10^{-12}
Sewage efficiency (%)	93%	97%	96%	89%	98%

Table 5. Comparison of the efficiency of sewage discharge (cough with mask).

Name	General Model	Optimization Scheme 1	Optimization Scheme 2	Optimization Scheme 3	Optimization Scheme 4
t = 0.50 s droplets concentration(kg/m^3)	1.16×10^{-10}		1.16×10^{-10}		
t = 120 s droplets concentration(kg/m^3)	1.5990×10^{-11}	1.5845×10^{-11}	9.8852×10^{-12}	1.0467×10^{-11}	1.4101×10^{-11}
Sewage efficiency (%)	86%	86%	92%	91%	88%

The sewage efficiency needs to be higher than 93% and 86%, respectively, in the case of wearing a mask and without a mask to be called superior. In Figure 20a, schemes 1, 2 and 4 can all outperform the sewage efficiency of the general model. Only scheme 3 is lower than the sewage discharge efficiency of the general model. At this time, the concentration of droplets in the negative pressure isolation cabin is 10.0306×10^{-12} kg/m^3, which is higher than the simulation results of the other four groups. The simulation results of the four sets of optimization schemes in Figure 20b are better than the simulation results of the general model, among which the simulation results of scheme 1 are basically the same as those of the general model. The sewage efficiency of scheme 2 is the best under this working condition, which can reach 92%.

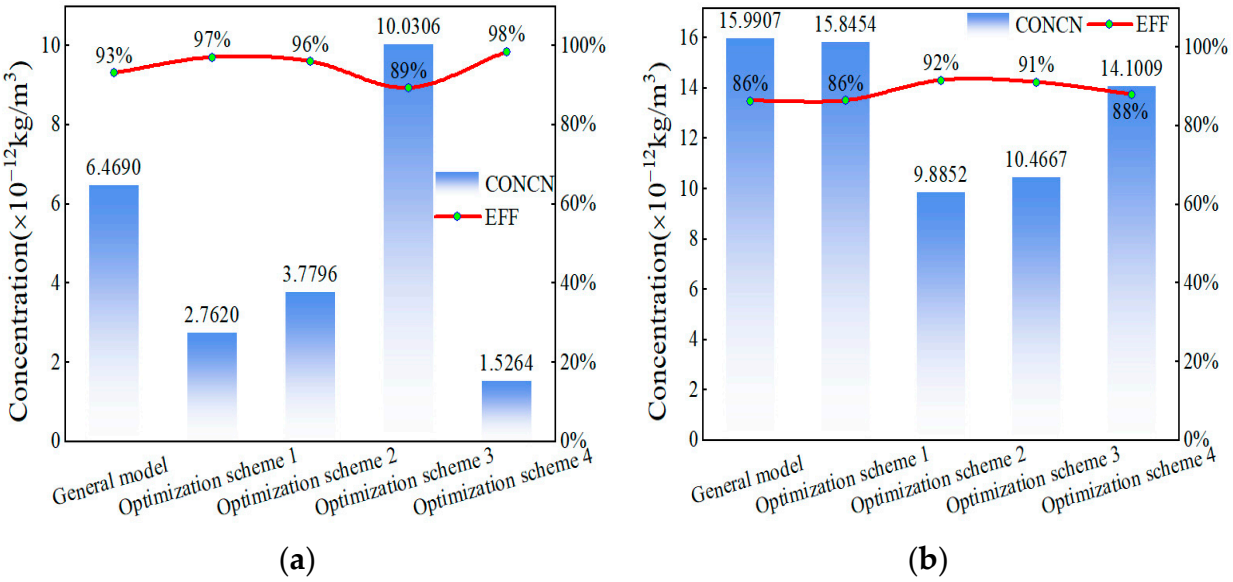

Figure 20. Comparison diagram of droplets particle concentration and sewage discharge efficiency (**a**) no masks; (**b**) with mask.

5. Infection Risk Assessment

In addition to judging the flow of droplets from the patient's cough and the discharge efficiency of the entire watershed system, another important index is the assessment of infection risk. Although the negative pressure isolation cabin is better at protecting medical staff and the external environment than a general isolation cabin, its internal structure is complicated and the airflow direction is more chaotic. The medical staff in the cabin remain in a prolonged and highly hazardous environment. Currently, there are four known transmission routes of droplets, among which contact transmission and aerosol transmission are the most common in the process of facilitating the isolation of patients in the isolation cabin [35]. Therefore, this study divided the risk area into two parts: human surface and respiratory area, and analyzed the infection risk from two aspects: contact transmission and aerosol transmission.

5.1. Risk Assessment of Contact-Borne Infections

We analyzed the infection risk to the medical staff accompanying the patient in the negative pressure isolation cabin, including one caregiver and two individuals. The collected droplet particle data included the number of droplets contained on the body surface of the three medical staff, so that the dose relationship of the simulation results could be accurately obtained. After analysis, a linear quantitative evaluation model is adopted to assess the infection risk of possible contact transmission patterns on the body surface of medical personnel [36]:

$$R_j = \sum R_{i,j} = \sum \frac{C_i N_{i,j}}{N_0} \quad (5)$$

where R_j is the total infection risk of the medical staff j. $R_{i,j}$ are single risks, which are multiplied by the number of viruses collected that may cause infection $N_{i,j}$, and the risk factor C_i. N_0 is the baseline number of infection risk and the value is 500.

In order to accurately calculate the risk of infection on the human surface, the droplet virus particles trapped on the human surface are divided into two regions, which are sorted according to the variable I of Equation (5) [36]:

When I = 1, the value is the number of droplets captured by the face of the medical staff. Since the droplets are very close to the mouth and nose of medical staff, the value is 1.

When I = 2, the value is the number of droplets captured on the surface of the medical staff. At this time, medical staff will be infected with the virus through contact with clothing or skin, and there is a risk of sensitization, the value is 0.1.

When I = 3, the value is the number of virus particles on the floor of the carriage. Although the simulation process ignores the factor of human movement, the droplets settled on the ground will still blow up again due to the air flow and the bumps of the car's driving process, with a value of 0.01.

According to Equation (5), the risk of human surface infection is calculated in five groups of models, including the general model, as shown in Figure 21. In Figure 21a, a patient without a mask can produce a very high number of virus-carrying droplets, and the risk of infection does not exceed 7% in all protocols. In the first scheme, the risk of infection by caregiver and individuals carrying the virus through the human surface is the largest, both greater than that of the general model. The total risk of infection can reach 6.59%, and the risk of infection of caregiver is the highest. The overall infection risk of scheme 2 is lower than that of the general model and the total infection risk value was 3.75%. Scheme 3 has the lowest total infection risk, only 3.99%. The overall infection risk in scheme 4 is smaller than that of the general model, but the total individual infection risk is higher than that of the general model. In Figure 21b, the patient wearing a mask can effectively reduce the number of droplets produced, greatly reduce the intensity of airflow generated by the patient's breathing mode, and also greatly reduce the chance of infection of medical staff. Both scheme 1 and scheme 4 reduce the chance of infection to 0% for all medical staff under these conditions.

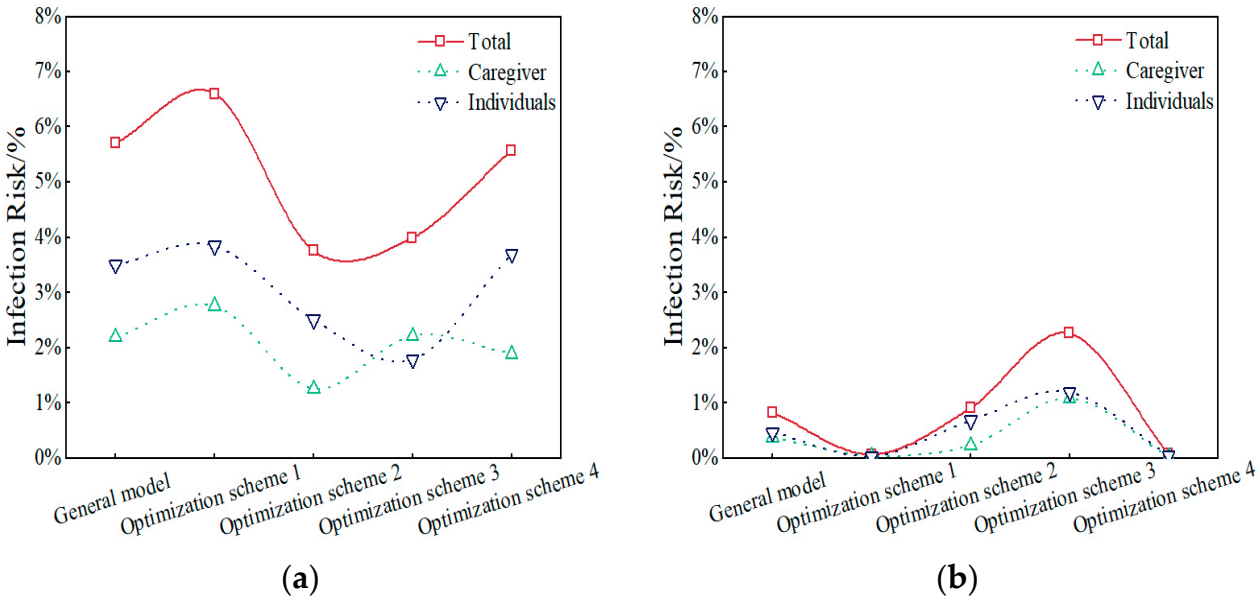

Figure 21. Risk of contact transmitted infections (**a**) without masks; (**b**) with mask.

5.2. Risk Assessment of Aerosol-Borne Infections

The dose–response model was first used to assess the risk of tuberculosis infection. The EPA's four-step model of population health risk assessment defines the model as describing the likelihood and severity of adverse health effects at a certain dose and exposure to a chemical. In 2008, Sze To et al. proved the potential application of the viability function of airborne viral pathogens in exposure assessment and infection risk analysis, and obtained the exposure estimation method [37], which is expressed as:

$$b(x_i, t_0) = cp \int_0^{t_0} v(x_i, t_0) f(t) dt \quad (6)$$

where c is the initial pathogen concentration; p is the respiration volume, m^3/h; v (x_i, t_i) is the concentration of virus volume that varies over time in x_i, the volume fraction of the pathogen m particle size pathogen; and $f(t)$ is the pathogen's survivability parameter.

Finally, based on the exponential dose–response model, a risk model containing estimated pathogen exposure is proposed. The sorted formula of the random non-threshold dose–response model is expressed as follows [37]:

$$P_I(x_i, t_i) = 1 - e^{-\sum_{m=1}^{n} r_m \beta_m cpq \int_0^{t_i} v(x_i,t)_m f(t) dt} \quad (7)$$

where P_I (x_i, t_i) is the probability of infection or the risk of infection at the x_i position within t_i time; t_i is the exposure time, h; m is the total number of pathogens; r_m is the infectious parameter of the m particle size pathogen; β_m is the percentage of exposure of the m particle size pathogen at the target site; and q is the frequency of coughing.

From Equation (7) above, it can be seen that the model is used to evaluate the virus collected over time at x_i position, while the aerosol droplets mentioned in this paper are dispersed in the drainage basin of the negative pressure isolation cabin. Although many droplets are produced when the patient does not wear a mask, the concentration of aerosol particles in the entire basin is not very high, so analyzing the risk value of infection at one point cannot fully reflect the risk value of infection of medical staff. After comprehensive consideration, in order to obtain more accurate and effective risk assessment result data, it is necessary to improve the theoretical basis of the dose–response model.

The MSDR model (Medical Staff Dose–response infection Risk Assessment Model) is improved on the basis of dose–response model, which can further analyze the influence of air flow organization factors on the infection risk of medical staff. It is a quantitative evaluation mechanism for the infection risk of medical staff [38,39].

According to the characteristics of MSDR model, Equation (6) is modified as follows:

$$E(z, t_l) = cp \sum_{i=1}^{l} \sum_{k=1}^{n} \frac{4\pi d_{0k}^3 f(t) \Delta t_i}{3HS} \quad (8)$$

where E (z, t_l) is the exposure evaluation model of a single droplet particle in the respiratory region within the time step l; d_{0k} is the diameter of the k droplets, m; Δt_i is the I time step; H is the vertical height of the respiratory area, 0.2 m [40]; and S is the horizontal area of the medical personnel breathing in the isolation cabin, $S_{0.60}$ = 4.58 m^2, $S_{1.05}$ = 4.87 m^2, $S_{1.45}$ = 4.66 m^2.

The MSDR model is obtained by modifying on the basis of Equation (7), and the expression is:

$$P_I(z, t_l) = 1 - \exp\left(-\sum_{j=1}^{m} r_j \beta_j cp \sum_{i=1}^{l} \sum_{k=1}^{n} \frac{4\pi d_{0k}^3 f(t) \Delta t_i}{3HS} \right) \quad (9)$$

In the formula, when $d_{0k} \leq 3$ μm, the infection parameter of the j pathogen r_j = 0.387, otherwise r_j = 0.0031. The percentage of the j particle size pathogen exposed at the target site $\beta_j = 2.587e^{-0.819 d_p}$. Pathogen survival parameters $f(t) = 0.2\ (0.975)^{\frac{t}{60}}$. The initial concentration c was 1×10^5 $TCID_{50}/mL$ [41]. The respiratory volume p was 8.6 L/min.

(1) No mask infection risk assessment

As shown in Figure 22, the result of the infection risk when medical staff is standing is shown in Figure 22a. The infection risk of the five groups increased rapidly before 12 s, and the value was in the range of 0.25963~0.07923. The risk value of infection in scheme 1 and scheme 4 is 2~3 higher than that of the general model. The infection risk value of scheme 2 and the general model is basically equal, and the infection risk value of scheme 3 is the lowest. The infection risk of medical staff while sitting is shown in Figure 22b. The infection risk of the five groups increased rapidly in the extreme time, and basically stabilized after 12 s, with an infection risk value ranging from 0.28051 to 0.18275. All optimizations have

lower infection risk values than the general model. Scheme 2 and scheme 3 performed best. The infection risk of medical staff at work are shown in Figure 22c. The overall risk values of infection in this region were small, ranging from 0.00222 to 0.00292. The infection risk values of scheme 1, scheme 2 and scheme 3 were all lower than those of the general model. Under normal sitting conditions, the risk of infection in scheme 2 decreased by 34.85%.

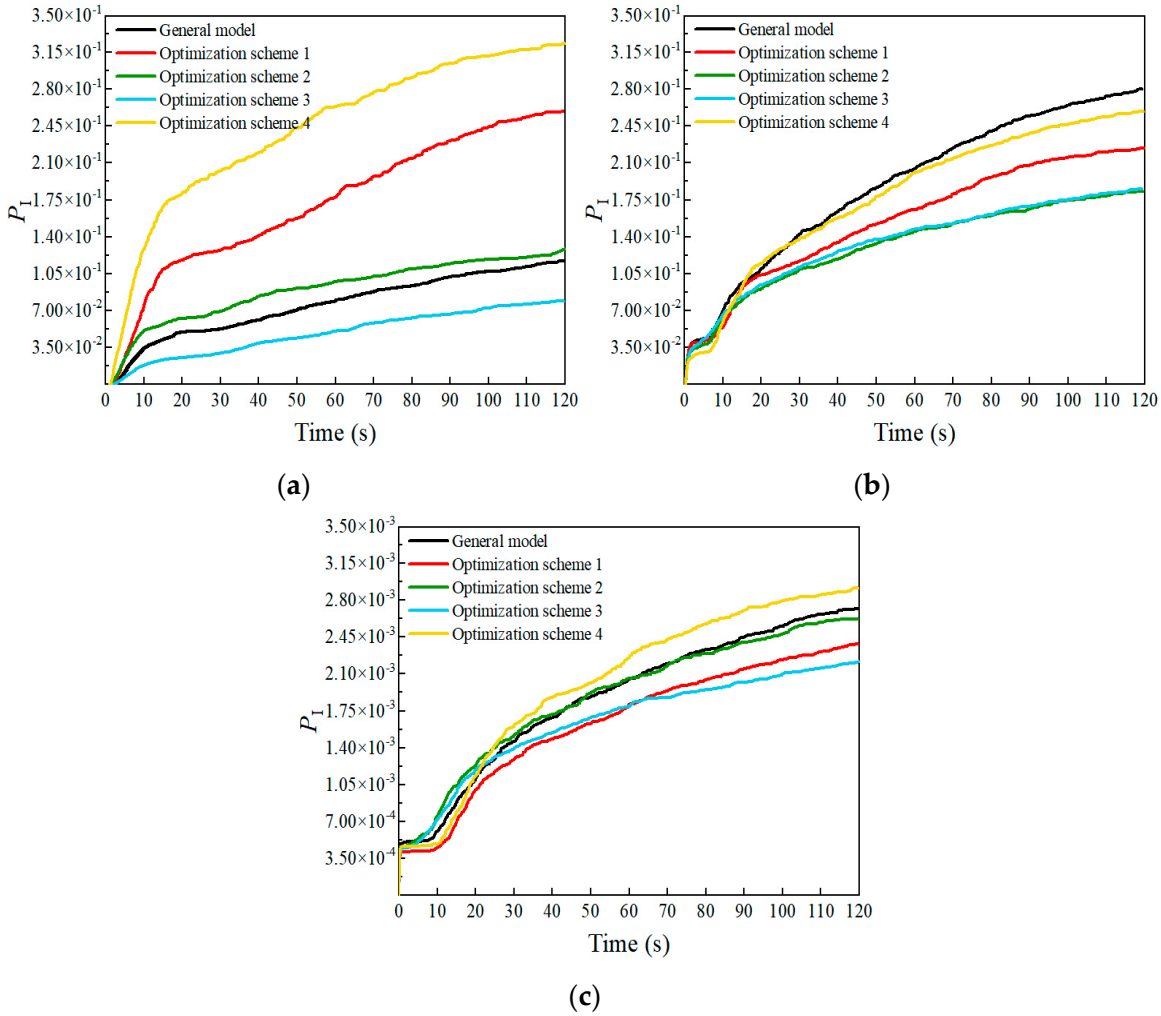

Figure 22. Risk of infection in different respiratory areas (cough without mask) (**a**) Z = 1.45 m; (**b**) Z = 1.05 m; (**c**) Z = 0.60 m.

(2) Infection risk assessment by wearing a mask

This is shown in Figure 23. The infection risk result when the caregiver is standing is shown Figure 23a. The infection risk value of the general model is 0.00590. Except for the third scheme, the infection risk value of other optimized schemes is lower than that of the general model. The result of the infection risk of the medical staff sitting is Figure 23b. The overall infection risk value is much smaller than that of Figure 23a, but the change trend is basically the same. The results of the infection risk at work for medical staff is shown in Figure 23c. The infection risk value in the general model is 1.11982×10^{-4}. Although the effect of schemes 2 and 3 is worse than that of the general model, their infection risk values are of the same order of magnitude as that of the general model, and the change is not great, and the best effect is scheme 4. The infection risk value is only 1.54398×10^{-9}. Since it has been mentioned in this paper that it is possible for patients to wear masks or not, from the perspective of infection risk assessment, the optimal scheme is finally selected as scheme 2. With normal sitting posture, the risk of infection is reduced by 71.77%.

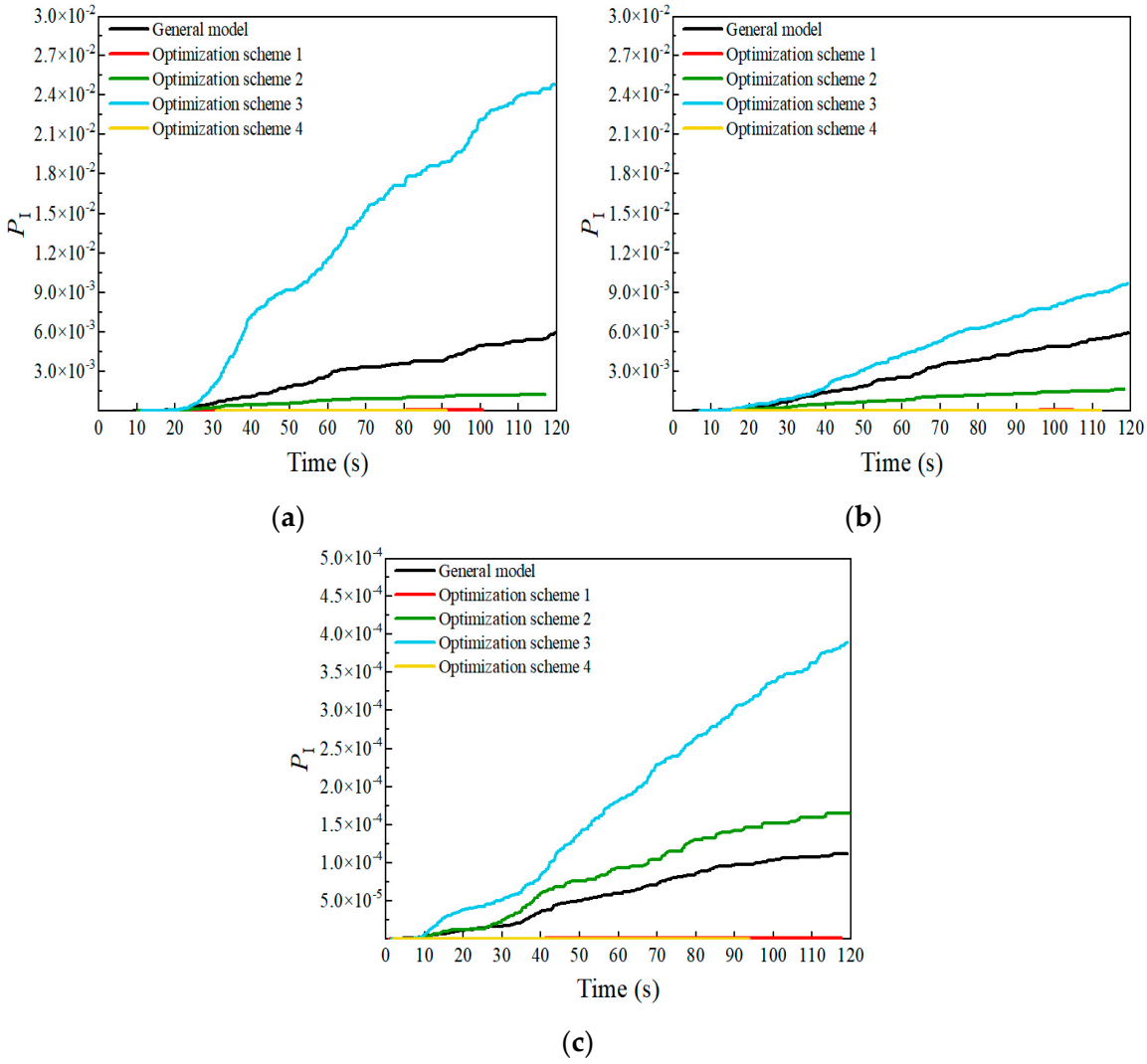

Figure 23. Risk of infection in different respiratory areas (cough with mask) (**a**) Z = 1.45 m; (**b**) Z = 1.05 m; (**c**) Z = 0.60 m.

6. Conclusions

As an important tool to prevent aerosol-borne diseases and to protect medical staff, the complex flow field structure in the negative pressure isolation cabin cannot be ignored. Optimizing the internal structure of the isolation cabin is of great significance for the prevention and treatment of infectious diseases. According to the research content of this paper, the main conclusions are as follows:

(1) Based on the principle of active interference, auxiliary air inlets are added above or behind the faces of caregiver and individuals, and four sets of optimization schemes are proposed. The diffusion of droplets generated by the three respiratory modes of coughing, sneezing, and talking by patients in the general model is simulated, and the residence time and particle size distribution of droplets in the basin are compared and analyzed with or without the patient wearing a mask. The results show that the medical staff in the negative pressure isolation cabin have different degrees of exposure risk.

(2) The common cough breathing mode in COVID-19 is analyzed and the superiority of optimal scheme 2 is demonstrated by comparing its droplet particle destination and pollutant discharge efficiency. Compared to the general model, the sewage efficiency of the scheme is increased by 3% when the patient wears a mask and 6% when the

patient does not wear a mask. The sewage efficiency, as a reference data, is 96% and 92% without and with masks, respectively.

(3) The risk of infection is evaluated from the aspects of contact transmission and aerosol transmission. The linear quantitative evaluation model and MSDR model are used to evaluate these transmission risks, respectively, and the results again show that optimization scheme 2 is the best. Compared with the general model, the risk of infection without mask is reduced by 34.85% and the risk of infection with mask is reduced by 71.77%. These results indicate the importance of structural optimization of the negative pressure isolation cabin of large cruise ships.

The results of this paper have limitations to a certain extent because the droplets produced by human coughing and other breathing methods contain sodium, potassium, and other elements, and the failure to refine the droplet parameters will cause deviations in the calculated results. Due to various factors, the relevant experiments have not been carried out, resulting in the simulation results not being compared and analyzed with the experimental data, and the parameter correction link is missing. Under the influence of many factors, it is still necessary to explore new methods and new ideas to study and improve the special isolation tool of the negative pressure isolation cabin in cruise ships.

Author Contributions: Conceptualization, X.L., Y.Z. and S.Z.; methodology, X.L. and S.Z.; software, X.L.; validation, X.L. and Y.Z.; formal analysis, X.L.; investigation, X.L., Y.Z. and S.Z.; resources, S.Z.; data curation, X.L.; writing—original draft preparation, X.L. and Y.Z.; writing—review and editing, S.Z. and Y.Z.; visualization, X.L.; supervision, S.Z.; project administration, S.Z.; funding acquisition, S.Z. All authors have read and agreed to the published version of the manuscript.

Funding: The research is partially funded by National Key R&D Program of China (No. 2017YFC0804805).

Institutional Review Board Statement: Not applicable.

Informed Consent Statement: Not applicable.

Data Availability Statement: Not applicable.

Conflicts of Interest: The authors declare no conflict of interest.

References

1. Kordsmeyer, A.C.; Mojtahedzadeh, N.; Heidrich, J.; Militzer, K.; von Münster, T.; Belz, L.; Jensen, H.J.; Bakir, S.; Henning, E.; Heuser, J.; et al. Systematic review on outbreaks of SARS-CoV-2 on cruise, navy and cargo ships. *Int. J. Environ. Res. Public Health* **2021**, *18*, 5195. [CrossRef]
2. Mccarter, Y.S. Infectious Disease Outbreaks on Cruise Ships. *Clin. Microbiol. Newsl.* **2009**, *31*, 161–168. [CrossRef]
3. Cramer, E.H.; Slaten, D.D.; Guerreiro, A.; Robbins, D.; Ganzon, A. Management and control of varicella on cruise ships: A collaborative approach to promoting public health. *Travel Med.* **2012**, *19*, 226–232. [CrossRef]
4. Newsom, R.; Amara, A.; Hicks, A.; Quint, M.; Pattison, C.; Bzdek, B.; Burridge, J.; Krawczyk, C.; Dinsmore, J.; Conway, J. Comparison of droplet spread in standard and laminar flow operating theatres: SPRAY study group. *J. Hosp. Infect.* **2021**, *110*, 194–200. [CrossRef]
5. Jain, A.; Dai, T.B.K.; Myers, C.G. COVID-19 created an elective surgery backlog: How can hospitals get back on track. *Harv. Bus. Rev.* **2020**, *10*, 1–7.
6. Outbreak Updates for International Cruise Ships. Available online: https://www.cdc.gov/nceh/vsp/surv/gilist.htm (accessed on 14 August 2023).
7. Liu, X.; Chang, Y.C. An emergency responding mechanism for cruise epidemic prevention—Taking COVID-19 as an example. *Mar. Policy* **2020**, *119*, 104093. [CrossRef]
8. Hung, I.F.N.; Cheng, V.C.C.; Li, X.; Tam, A.R.; Hung, D.L.L.; Chiu, K.H.Y.; Yip, C.C.Y.; Cai, J.P.; Ho, D.T.Y.; Wong, S.C.; et al. SARS-CoV-2 shedding and seroconversion among passengers quarantined after disembarking a cruise ship: A case series. *Lancet Infect. Dis.* **2020**, *9*, 1051–1060. [CrossRef]
9. Binns, P.L.; Sheppeard, V.; Staff, M.P. Isolation and quarantine during pandemic (H1N1) 2009 influenza in NSW: The operational experience of public health units. *NSW Public Health Bull* **2010**, *21*, 10–15. [CrossRef]
10. Rocklv, J.; Sjdin, H.; Wilder-Smith, A. COVID-19 outbreak on the Diamond Princess cruise ship: Estimating the epidemic potential and effectiveness of public health countermeasures. *J. Travel Med.* **2020**, *3*, taaa030. [CrossRef] [PubMed]
11. Lindsley, W.G.; Blachere, F.M.; Law, B.F.; Beezhold, D.H.; Noti, J.D. Efficacy of face masks, neck gaiters and face shields for reducing the expulsion of simulated cough-generated aerosols. *Aerosol Sci. Technol.* **2021**, *55*, 449–457. [CrossRef] [PubMed]

12. Li, H.; Meng, S.; Tong, H. How to control cruise ship disease risk? Inspiration from the research literature. *Mar. Policy* **2021**, *132*, 104652. [CrossRef]
13. China News. Negative Pressure Isolation Room Officially Opened at Tianjin Dongjiang Cruise Ship Homeport. Available online: http://www.chinanews.com/df/2014/09--14/6589182.shtml (accessed on 14 August 2023).
14. Zhang, Z.; Chen, Q. Particle dispersion in a room with under-floor air distribution. *Proc. Indoor Air* **2005**, *3*, 2723–2728.
15. Zhu, S.; Kato, S.; Yang, J.H. Study on transport characteristics of saliva droplets produced by coughing in a calm indoor environment. *Build. Environ.* **2006**, *41*, 1691–1702. [CrossRef]
16. Noh, K.C.; Kim, H.S.; Oh, M.D. Study on contamination control in a minienvironment inside clean room for yield enhancement based on particle concentration measurement and airflow CFD simulation. *Build. Environ.* **2010**, *45*, 825–831. [CrossRef]
17. Wan, M.P.; Chao, C.Y.H.; Ng, Y.D.; To, G.N.S.; Yu, W.C. Dispersion of expiratory droplets in a general hospital ward with ceiling mixing type mechanical ventilation system. *Aerosol Sci. Technol.* **2007**, *41*, 244–258. [CrossRef]
18. Qian, H.; Li, Y.; Nielsen, P.V.; Huang, X. Spatial distribution of infection risk of SARS transmission in a hospital ward. *Build. Environ.* **2009**, *44*, 1651–1658. [CrossRef]
19. Qi-Bin, H.E.; Nai-Ping, G.; Tong, Z. Using CFD Method to Simulate Aerosol Particle Dispersion and Deposition in Enclosed Environment. *Build. Energy Environ.* **2010**, *1*, 26–31.
20. Kwon, S.-B.; Park, J.; Jang, J.; Cho, Y.; Park, D.-S.; Kim, C.; Bae, G.-N.; Jang, A. Study on the initial velocity distribution of exhaled air from coughing and speaking. *Chemosphere* **2012**, *87*, 1260–1264. [CrossRef]
21. Vuorinen, V.; Aarnio, M.; Alava, M.; Alopaeus, V.; Atanasova, N.; Auvinen, M.; Balasubramanian, N.; Bordbar, H.; Erästö, P.; Grande, R. Modelling aerosol transport and virus exposure with numerical simulations in relation to SARS-CoV-2 transmission by inhalation indoors. *Saf. Sci.* **2020**, *130*, 104866. [CrossRef]
22. Saw, L.H.; Leo, B.F.; Nor, N.S.M.; Yip, C.W.; Ibrahim, N.; Hamid, H.H.A.; Latif, M.T.; Lin, C.Y.; Nadzir, M.S.M. Modeling aerosol transmission of SARS-CoV-2 from human-exhaled particles in a hospital ward. *Environ. Sci. Pollut. Res.* **2021**, *28*, 53478–53492. [CrossRef]
23. Kennedy, M.; Lee, S.J.; Epstein, M. Modeling aerosol transmission of SARS-CoV-2 in multi-room facility. *J. Loss Prev. Process Ind.* **2021**, *69*, 104336. [CrossRef] [PubMed]
24. Jeong, D.; Yi, H.; Park, J.-H.; Park, H.W.; Park, K. A vertical laminar airflow system to prevent aerosol transmission of SARS-CoV-2 in building space: Computational fluid dynamics (CFD) and experimental approach. *Indoor Built Environ.* **2022**, *31*, 1319–1338. [CrossRef]
25. Pletcher, R.H.; Tannehill, J.C.; Anderson, D. *Computational Fluid Mechanics and Heat Transfer*; Markatos, N.C., Ed.; CRC Press: Boca Raton, FL, USA, 2012; pp. 247–252.
26. Kumar, R.; Gopireddy, S.R.; Jana, A.K.; Patel, C.M. Study of the discharge behavior of Rosin-Rammler particle-size distributions from hopper by discrete element method: A systematic analysis of mass flow rate, segregation and velocity profiles. *Powder Technol.* **2020**, *360*, 818–834. [CrossRef]
27. Dbouk, T.; Drikakis, D. On respiratory droplets and face masks. *Phys. Fluids* **2020**, *32*, 063303. [CrossRef]
28. Bhat, S.P.; Kumar, B.V.; Kalamkar, S.R.; Kumar, V.; Pathak, S.; Schneider, W. Modeling and simulation of the potential indoor airborne transmission of SARS-CoV-2 virus through respiratory droplets. *Phys. Fluids* **2022**, *34*, 031909. [CrossRef]
29. Shang, Y.; Dong, J.; Tian, L.; He, F.; Tu, J. An improved numerical model for epidemic transmission and infection risks assessment in indoor environment. *J. Aerosol Sci.* **2022**, *162*, 105943. [CrossRef]
30. Unno, T. Aerodynamics of Sneezing. *Auris Nasus Larynx* **1975**, *2*, 17–27. [CrossRef]
31. Bourouiba, L. A Sneeze. *N. Engl. J. Med.* **2016**, *375*, e15. [CrossRef]
32. Tsang, T.W.; Mui, K.W.; Wong, L.T. Computational Fluid Dynamics (CFD) studies on airborne transmission in hospitals: A review on the research approaches and the challenges. *J. Build. Eng.* **2022**, *63*, 105533. [CrossRef]
33. Karkoulias, D.G.; Tzoganis, E.D.; Panagiotopoulos, A.G.; Acheimastos, S.-G.D.; Margaris, D.P. Computational Fluid Dynamics Study of Wing in Air Flow and Air–Solid Flow Using Three Different Meshing Techniques and Comparison with Experimental Results in Wind Tunnel. *Computation* **2022**, *10*, 34. [CrossRef]
34. Qian, H.; Li, Y.; Nielsen, P.V.; Hyldgaard, C.E.; Wong, T.W.; Chwang, A.T. Dispersion of exhaled droplet nuclei in a two-bed hospital ward with three different ventilation systems. *Indoor Air* **2010**, *16*, 111–128. [CrossRef] [PubMed]
35. Wang, Y.; Liu, Z.; Liu, H.; Wu, M.; He, J.; Cao, G. Droplet aerosols transportation and deposition for three respiratory behaviors in a typical negative pressure isolation ward. *Build. Environ.* **2022**, *219*, 109247. [CrossRef] [PubMed]
36. Wu, J.L.; Weng, W.G. Transmission of COVID-19 viral particles and the risk of infection among passengers in air-conditioned buses. *J. Tsinghua Univ. Sci. Technol.* **2021**, *61*, 89–95. (In Chinese)
37. To, G.N.S.; Wan, M.P.; Chao, C.Y.H.; Wei, F.; Yu, S.C.T.; Kwan, J.K.C. A methodology for estimating airborne virus exposure in indoor environments using the spatial distribution of expiratory aerosols and virus viability characteristics. *Indoor Air* **2008**, *18*, 425–438.
38. Bale, R.; Iida, A.; Yamakawa, M.; Li, C.; Tsubokura, M. Quantifying the COVID19 infection risk due to droplet/aerosol inhalation. *Sci. Rep.* **2022**, *12*, 11186. [CrossRef]
39. Guo, X.L. Study on the Evaporation and Diffusion Law of Cough Droplets and the Evaluation of Infection Risk under the Influence of Airflow. Master's Thesis, Huazhong University of Science &Technology, Wuhan, China, 2020. (In Chinese)

40. Xie, J.L.; Wu, X.; Guo, X.L.; Hou, J.X.; Duan, M.Z.; Wang, F.F.; Xu, X.H.; Gao, N.P. Simulation of air distribution in isolation ward based on infection risk assessment model. *J. Cent. South Univ. Sci. Technol.* **2021**, *52*, 1798–1808. (In Chinese)
41. Zhou, S.W.; Zhang, L.W. Research on Airflow Optimization and Infection Risk Assessment of Medical Cabin of Negative-Pressure Ambulance. *Sustainability* **2022**, *14*, 4900. [CrossRef]